Mon. Not. R. Astron. Soc. **307**, 857–876 (1999)

Chemo-spectrophotometric evolution of spiral galaxies – I. The model and the Milky Way

S. Boissier and N. Prantzos★
Institut d'Astrophysique de Paris, 98bis Bd. Arago, 75014 Paris, France

Accepted 1999 March 19. Received 1999 March 1; in original form 1998 November 30

ABSTRACT

The chemical and spectrophotometric evolution of spiral galaxies is investigated with detailed models, making use of up-to-date ingredients (like metallicity-dependent stellar properties) and a prescription for the star formation rate (SFR) justified both empirically and theoretically. As a first application, the model is used to describe the evolution of the Milky Way. The role of the adopted scheme of disc formation ('inside-out') in shaping the various chemical and colour profiles is investigated, as well as the role of extinction. It is shown that the Solar neighbourhood does not evolve like the Milky Way as a whole and that one-zone models with a non-linear SFR prescription cannot be used to study the evolution of our Galaxy. Our model average SFR is shown to match well observations of external spirals.

Key words: Galaxy: evolution – Galaxy: general – Galaxy: structure – galaxies: evolution – galaxies: photometry – galaxies: spiral.

1 INTRODUCTION

Galactic evolution is one of the major topics of research in modern astrophysics. Despite more than three decades of intense observational and theoretical studies, the subject has not yet reached the maturity of other fields, like e.g. stellar evolution. Our limited understanding of the 'driver' of galactic evolution, i.e. star formation from the interstellar medium, is the main reason for this situation.

Galactic discs are privileged places for the study of the star formation rate (SFR) since their various properties (surface densities of stars and gas, SFR, abundances of various elements, luminosity and colour profiles, etc.) can be measured as a function of galactocentric distance and compared to theoretical predictions. Notice that predictions for the SFR exist only for disc galaxies (based on various instability criteria, e.g. Talbot & Arnett 1975; Onihishi 1975; Wyse & Silk 1989; Dopita & Ryder 1994), not for ellipticals or irregulars. Testing these predictions against the largest observational data set is obviously crucial for our understanding of the SFR.

Until recently, detailed observed properties of disc galaxies were available only for the local Universe, i.e. at very low redshift. These data offer information only about the current status of galaxies, from which their past history is to be derived; in view of the many model parameters, it is difficult to deduce a unique history from those data (in one single case, namely the Milky Way, we have information on the local disc history, via the age–metallicity relationship and the metallicity distribution of low-mass stars). The spectacular progress in instrumentation now makes possible the observation of galaxy morphology at higher redshifts (e.g. Lilly et al. 1998) and will soon allow one to compare models to observations covering the largest part of galaxy evolution.

The various aspects of galactic evolution, namely dynamical, chemical and spectrophotometric, have usually been treated separately up to now (with a few exceptions). A large number of multizone chemical evolution models have been proposed, matching in a relatively satisfactory way the current chemical properties of the Milky Way disc (e.g. Matteucci & François 1989; Ferrini et al. 1994; Prantzos & Aubert 1995; Carigi 1996; Tosi 1998; Dwek 1998) or the (much less constraining) chemical profiles of external spirals (e.g. Molla, Ferrini & Diaz 1997); in some cases, this class of models takes into account the possibility of radial flows of gas in the galactic discs (e.g. Mayor & Vigroux 1981; Lacey & Fall 1985; Clarke 1989; Tsujimoto et al. 1995; Firmani, Hernandez & Tutukov 1996). On the other hand, one-zone spectrophotometric evolution models (treating the whole galaxy as one single region) have been developed, matching the integrated photometric properties of spirals along the Hubble sequence (usually varying the SFR time-scale, e.g. Guiderdoni & Rocca-Volmerange 1987; Arimoto, Yoshii & Takahara 1992; Bruzual & Charlot 1993); these models do not provide a detailed study of the chemical properties or of the photometric gradients in spirals. Preliminary multizone chemo-photometric evolution models have been studied by Talbot & Arnett (1975), while more recent ones were applied to low surface brightness galaxies (e.g. Jimenez et al. 1998).

Chemo-dynamical evolution models have been developed and applied to spirals by a few groups (Steinmetz & Muller 1994; Samland, Hensler & Theis 1997); these models have a less sophisticated treatment of chemical evolution than the classical ones and are still subject to the uncertainties of initial conditions

★ E-mail: prantzos@iap.fr

and gas–stars interactions. In a recent work, Contardo, Steinmetz & Fritze-von Alvesleben (1998) made the first attempt, to our knowledge, to combine in a single computation photometry, chemistry and dynamics; despite the failure to reproduce basic observational properties of the Milky Way disc (like the local G-dwarf metallicity distribution – see Section 3.1.1 – or colour gradients at low redshifts), this type of model seems quite promising and shows the way that galactic evolution studies should go in the future; however, in view of the large and many uncertainties affecting dynamical models (and their coupling to chemistry) at present, the road to convincing unified treatment is expected to be rather long.

This paper is the first of a series aiming to study in a unified framework the chemical *and* spectrophotometric properties of spiral galaxies, with appropriate detailed multizone models. Here we present in some detail the model and its application to the Milky Way, which will serve as a 'template' for further studies. In Section 2.1 we present the chemical evolution part of the model, justifying our choice of the adopted SFR law (Section 2.1.2) In Section 2.2 we present the spectrophotometric part of the model, emphasizing the homogeneity of the adopted sets of stellar tracks and spectra (both as a function of metallicity) and the importance of a correct treatment of metallicity-dependent stellar lifetimes in the calculation of the photometric evolution. In Section 3.1 we present the results of the model for the chemical and photometric evolution of the Solar neighbourhood and study the effects of metallicity-dependent ingredients and of extinction on those results. In Section 3.2 we present the results for the Milky Way disc and we discuss the evolution of the various chemical and photometric gradients and the (limited) role of extinction in shaping the latter; we also discuss the populations of stellar remnants and their role on various aspects of studies of the Galaxy. In Section 3.3 we compare the evolution of the Solar neighbourhood to the one of the Milky Way as a whole and show that they differ considerably, i.e. one-zone models reproducing the local disc properties cannot be used to simulate the evolution of the whole Galaxy. In Section 3.4 we compare (favourably) the average SFR of the model with recent observations of the corresponding SFR in external spirals (from Kennicutt 1998). Finally, our main results are summarized in Section 4.

2 THE MODEL

2.1 Chemical evolution

The adopted model of galactic chemical evolution has been presented in previous works (i.e. Prantzos & Aubert 1995, hereafter PA95; Prantzos & Silk 1998, hereafter PS98). The classical set of the equations of galactic chemical evolution (Tinsley 1980; Pagel 1997) is solved numerically for each zone, without the instantaneous recycling approximation. Instantaneous mixing is assumed within each zone, i.e. at the death of the star its ejecta are thoroughly mixed in the local interstellar medium, which is characterized by a unique composition at any time (no abundance scatter is obtained in that framework). The main input physics of the model are described below.

2.1.1 *Stellar inputs: yields, remnant masses, lifetimes*

The yields of massive stars (i.e. the amount of stellar ejecta in the form of various elements) adopted in this work are those of Woosley & Weaver (1995, hereafter WW95) for metallicity $Z = Z_{\odot}$. Notice that in some cases they differ considerably from the corresponding ones of the other major recent work in the field (Thielemann, Nomoto & Hashimoto 1996). These differences are the result of the different physical inputs utilized by the two groups, mainly the criterion for convection, the nuclear reaction rates and the determination of the 'mass-cut' (see Prantzos 1998b for a review of the role of the yields of massive stars in chemical evolution). The most significant difference concerns the yields of Fe: in the case of WW95 they are increasing with stellar mass, while all massive stars eject $\sim 0.07\,M_{\odot}$ of Fe in the case of Thielemann et al. (1996).

For the masses of the stellar remnants we have adopted the following prescriptions. Stars with mass $M < 9\,M_{\odot}$ become white dwarfs with mass $M_{\rm R}(M/M_{\odot}) = 0.1M/M_{\odot} + 0.45$ (Iben & Tutukov 1984). Stars with $M > 8\,M_{\odot}$ explode as accretion-induced collapse (in the 8–11 $M_{\odot}$ range) or Fe core collapse (for $M > 11\,M_{\odot}$) supernovae, leaving behind a neutron star of mass $M_{\rm R} = 1.4\,M_{\odot}$ (as suggested by observations of neutron stars in binary systems, e.g. Thorsett & Chakrabarty 1999); the heaviest of those stars may form a black hole but the mass limit for its formation is not known at present and cannot be inferred from theoretical or observational arguments (e.g. Prantzos 1994; Bethe & Brown 1995), despite occasional claims to the contrary. Fortunately, owing to the steeply decreasing stellar initial mass function (IMF) in the range of massive stars (see Section 2.1.2), the mass limit for stellar black hole formation does not significantly affect the results of chemical evolution, at least as far as that limit is above $\sim 40\,M_{\odot}$. Attempts to determine the number and masses of galactic neutron stars and black holes based on the energetics of the supernova explosion and the Fe core mass have been made in Timmes, Woosley & Weaver (1996) and Bethe & Brown (1998); we feel, however, that the current understanding of these topics does not allow an accurate determination of those parameters and we adopt the aforementioned simple prescription, i.e. stars with $M > 8\,M_{\odot}$ leave a neutron star of $1.4\,M_{\odot}$, while stars of $M > 40\,M_{\odot}$ leave a black hole of $3\,M_{\odot}$ (obviously, the adopted values in the case of black hole formation are lower limits and they serve only for illustration purposes).

There are equally important uncertainties in the yields of $M < 9\,M_{\odot}$ stars, resulting from the treatment of mass loss, envelope convection, etc., especially in their final evolution on the asymptotic giant branch (AGB; see Charbonnel 1998 for a recent review). In this work we have adopted those of Marigo, Bressan & Chiosi (1996) in the range 1–4 $M_{\odot}$ and those of Renzini & Voli (1981) in the 4–9 $M_{\odot}$ range (their table 4d with hot bottom burning); despite the different physical inputs, the two sets of yields merge rather smoothly in the intermediate mass regime ($\sim 4\,M_{\odot}$). In any case, the uncertainties in those yields play a very limited role in the context of this work.

Finally, the adopted stellar lifetimes τ_M as a function of the stellar mass M are from the work of the Geneva group (Schaller et al. 1992; Charbonnel et al. 1996). The metallicity dependence of the stellar lifetimes (see Fig. 3) may affect considerably the results of photometric evolution (see Section 3.1.2).

2.1.2 *Stellar initial mass function (IMF)*

The choice of the IMF plays a crucial role in the results of chemical and photometric evolution of galaxies. Most photometric studies still use a Salpeter power-law IMF $\Phi(M) \propto M^{-(1+X)}$ with $X = 1.35$ in the whole stellar mass range, although Salpeter (1955) derived that IMF in the 0.6–10 $M_{\odot}$ range. However, several studies have shown that the IMF flattens below $M \sim 1\,M_{\odot}$ (e.g. Reid & Gizis 1997 and references therein) and the use of a

Salpeter IMF over the whole mass range (i.e. down to the H-burning limit) is in disagreement with observational evidence.

Although the flattening of the IMF below $\sim 1\,M_\odot$ is generally accepted now (e.g. Scalo 1998), its exact shape is still under debate. For instance, Reid & Gizis (1997), using a new sample of M dwarfs and an up-to-date mass–luminosity calibration, find that a single slope $X = 0.05$ can fit the whole mass range $0.1 < M/M_\odot < 1$. In a recent review, Kroupa (1998), after discussing all recent determinations of the low-mass part of the IMF, favours a slope $X = 0.5$ for $M < 0.5\,M_\odot$ and down to the H-burning limit.

On the other hand, the slope of the high-mass part of the IMF is also uncertain. Studies of OB associations on the Small and Large Magellanic Clouds (SMC, LMC) and the Milky Way (Massey, Johnson & Degioia-Eastwood 1995) show relatively flat slopes ($X \sim 1$–1.5). However, a surprisingly large number of massive stars (~ 50 per cent) are found outside OB associations according to Massey (1998), who finds that these 'field' stars have much steeper IMFs ($X \sim 3$–4 in the Milky Way, LMC and SMC). The slope of $X = 1.7$ suggested in Scalo (1986) seems a reasonable choice, on the basis of all available observational data (see Gilmore, Parry & Ryan 1998 and references therein).

The mass limits of the IMF also play an important role in the outcome of galactic evolution studies, in view of the normalization

$$\int_{M_{\rm min}}^{M_{\rm max}} \Phi(M) M \, {\rm d}M = 1 \qquad (1)$$

$M_{\rm max}$ is usually taken to be in the 50–$100\,M_\odot$ range and its exact value affects slightly the results of chemical evolution. The adopted $M_{\rm min}$ is usually $\sim 0.1\,M_\odot$ (i.e. close to the H-burning limit of $0.08\,M_\odot$) but lower values cannot be excluded provided they do not violate observational constraints. In the case of the solar neighbourhood, one such constraint is that the current surface density of brown dwarfs should not exceed $\sim 8\,M_\odot\,{\rm pc}^{-2}$ (Mera, Chabrier & Schaeffer 1998), i.e. ~ 15 per cent of the local surface density. A very small amount of brown dwarfs is also suggested by Reid & Gizis (1997), who find that their IMF drops below $\sim 0.1\,M_\odot$.

These considerations suggest that there is some freedom in the choice of the IMF. In our recent works (PA95; PS98) we adopted the IMF from the work of Kroupa, Tout & Gilmore (1993, hereafter KTG93), where the complex interdependence of several factors (like stellar binarity, ages and metallicities, as well as mass–luminosity and colour–magnitude relationships) is explicitly taken into account. It is a three-slope power-law IMF; in the high-mass regime it has a relatively steep slope of $X = 1.7$ (based on Scalo 1986), while it flattens in the low-mass range ($X = 1.2$ for $0.5 < M/M_\odot < 1$ and $X = 0.3$ for $M < 0.5\,M_\odot$). We adopt here again the KTG93 IMF between 0.1 and $100\,M_\odot$, although we are aware that there is some debate as to the exact form of the low-mass part (in view of the results of Gould, Bacall & Flynn 1997 and Reid & Gizis 1997; see, however, Haywood 1994). The KTG93 IMF is plotted in Fig. 1, where it is compared to the Salpeter IMF and the Reid & Gizis (1997) IMF. The KTG93 IMF has a smaller number of massive stars than the Salpeter IMF and so it produces less metals and Type II supernovae (SNII) (although the return mass fraction is similar in the two cases: ~ 0.30); on the other hand, it contains a larger number of intermediate and approximately Solar mass stars and thus produces more light than the Salpeter IMF (since it is precisely the long-lived 1–$2\,M_\odot$ stars that contribute most of the galactic light at late times). Notice that the IMF suggested by Reid & Gizis (1997, with $X = 0.05$ for $M < 1\,M_\odot$ and $X = 1.7$ for $M > 1\,M_\odot$) would produce even more light [when appropriately normalized, as in equation (1)]. These considerations have important implications for the chemo-spectrophotometric evolution of galaxies, which are rarely considered; in fact, most studies of photometric evolution adopt a Salpeter IMF in the whole mass range, without worrying about local observational evidence or implications for chemical evolution.

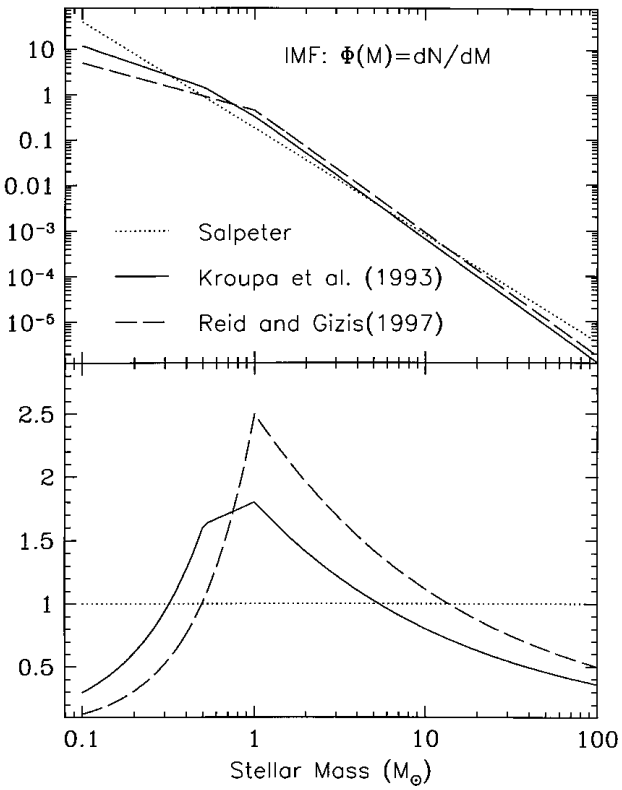

Figure 1. *Upper panel*: Initial mass functions (IMF), according to Salpeter (1995, *dotted* curve with a unique slope $X = 1.35$), Reid & Gizis (1997, *dashed* curve) and Kroupa et al. (1993, *solid* curve); the latter is adopted in this work. All curves are normalized according to equation 1 (see text). *Lower panel*: Ratio of the multislope IMFs to the Salpeter IMF; because of the normalization, they contain more intermediate- and low-mass stars and a smaller number of red dwarfs and massive stars.

Finally, the question of the variation of the IMF in time or space has not received a satisfactory answer for the moment, although most observers tend to favour the 'no variation' option. For instance, Massey et al. (1995) find no difference in the IMF of massive stars in OB associations between the SMC, LMC and the Milky Way, despite the factor of ~ 10 difference in metallicity between those regions; also, in a recent work Gizis & Reid (1999) find that the low-mass part of the IMF is the same in local disc and halo stars, i.e. independent of metallicity. On the other hand, Scalo (1998) rejects the 'myth of the universality of the IMF', on the basis of observational and theoretical arguments (for a thorough discussion of all aspects of the IMF see the volume edited by Gilmore et al. 1998).

2.1.3 *Star formation rate (SFR)*

The adopted star formation rate (SFR) Ψ is locally a Schmidt-type law $\Psi \propto \Sigma_{\rm G}^{1.5}$, where $\Sigma_{\rm G}$ is the local gas surface density. Such a proportionality has been suggested by Kennicutt (1989, 1998) on

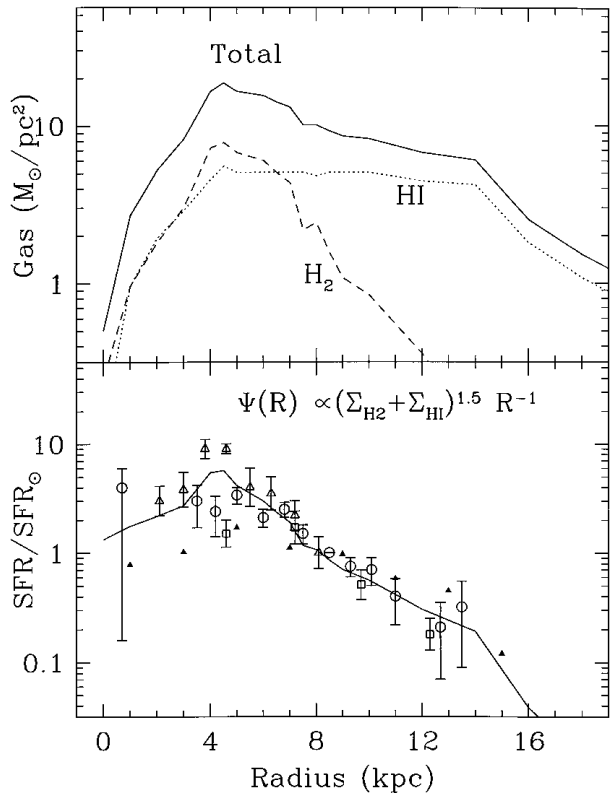

Figure 2. *Upper panel*: Current surface density profiles of molecular (H_2) and atomic (H I) hydrogen in the Milky Way, as a function of Galactocentric radius (from Dame 1993) and total gas surface density (the sum of the two, increased by 40 per cent to account for helium). *Lower panel*: Corresponding theoretical current SFR (*solid* curve, according to equation 2) and comparison to observational estimates of the current SFR profile. Data from: Lyne et al. (1985, open circles), Gusten & Mezger (1983, triangles), Guibert et al. (1978, squares). The SFR profiles are normalized to their value at $R_S = 8$ kpc.

the basis of observations of average SFR versus gas surface densities in spirals (see Section 3.4). On the other hand, a radial dependence of the star formation efficiency in disc galaxies is required in order to reproduce the observed gradients, and such a dependence has indeed been proposed on the basis of various instability criteria for gaseous discs (e.g. Talbot & Arnett 1975; Onihishi 1975; Wyse & Silk 1989; Dopita & Ryder 1994). It should be noted that star formation theories exist and may be tested mainly for disc galaxies, not for e.g. ellipticals or irregulars. We adopt in this work a star formation rate explicitly dependent on galactocentric radius. It is based on the idea that stars are formed in spiral galaxies when the interstellar medium with angular frequency $\Omega(R)$ is periodically compressed by the passage of the spiral pattern, having a frequency $\Omega_P = \text{constant} \ll \Omega(R)$. This leads to SFR $\propto \Omega(R) - \Omega_P \propto \Omega(R)$ and, for discs with flat rotation curves, to SFR $\propto R^{-1}$ (Wyse & Silk 1989), i.e.

$$\Psi(t,R) = 0.1\Sigma_G(R)^{1.5}(R/R_S)^{-1}\,M_\odot\,pc^{-2}\,Gyr^{-1} \quad (2)$$

where $R_S = 8$ kpc is the distance of the Sun to the Galactic centre. Such a radial dependence of the SFR is also compatible with observational evidence, as can be seen in Fig. 2, displaying the current gas surface density profile in the Milky Way disc (upper panel) and the corresponding SFR according to equation (2) (lower panel); comparison of this theoretical SFR to observations (lower panel in Fig. 2) shows a fairly good agreement. To our knowledge, this is the first time that this type of direct comparison has been pointed out. It has been shown that this form of the SFR can account for the observed gradients of gas fraction, SFR and chemical abundance profiles in the Milky Way (e.g. PS98 and Section 3.2.1). One of the major aims of the present work is to derive the corresponding photometric gradients (Section 3.2.2) and compare our model average SFR to recent observations concerning external spirals (Section 3.4).

2.1.4 *Supernova rates*

Once the SFR and IMF are fixed, and the lower mass limit M_{SNII} for the formation of Fe core collapse supernova is determined, the corresponding rate of SNII explosions can be calculated as

$$SNII(t) = \Psi(t)\int_{M_{SNII}}^{100\,M_\odot} \Phi(M)\,dM;$$

we adopt here $M_{SNII} = 8\,M_\odot$ (in fact, the most massive of these stars, as well as some of those in close binary systems, will suffer extensive mass losses prior to the explosion and appear as SNIb/c supernovae; but we keep the designation of SNII here for all core collapse events). With the adopted IMF, the integral in the formula above has the value 5.5×10^{-3}, i.e. 0.55 SNII century^{-1} are expected for a SFR of $1\,M_\odot\,yr^{-1}$; in the case of a Salpeter IMF, the corresponding number is slightly higher (7.7×10^{-3}).

On the other hand, a supplementary source of Fe peak nuclei is introduced in the form of Type Ia supernovae (SNIa), presumably white dwarfs in binary systems accreting material from their companion star (see Nomoto, Iwamoto & Kishimoto 1997 for a recent review of SNIa). The relative homogeneity of the observed SNIa light curves suggests that $\sim 0.7\,M_\odot$ of Fe are ejected (originally in the form of ^{56}Ni); this is also predicted by the most successful models of SNIa, involving carbon deflagration in a Chandrasekhar mass white dwarf. We adopt here the yields of the W7 model from Thielemann, Nomoto & Yokoi (1986). However, the evolution of the SNIa rate in the Galaxy is difficult to predict from the theory of binary systems alone (see e.g. Ruiz-Lapuente et al. 1997 and references therein). We adopt here the prescription of Matteucci & Greggio (1986), in order to reproduce the observed decline of O/Fe versus Fe/H in the local disc. Notice that the recent results of Israelian, Garcia-Lopez & Rebolo (1998) and Boesgaard et al. (1999) show a steady decline of that ratio also in halo stars, in disagreement with previous observations showing a 'plateau'; if these new results are confirmed, the SNIa rate formalism should be reconsidered.

The comparison of the model supernova rate (integrated over the disc) to observations of Milky Way type spirals (usually expressed in SNU, i.e. number of supernovae per century and per $10^{10}\,L_{B,\odot}$) is a crucial test of the model. It is feasible only in the framework of self-consistent models calculating both chemical *and* photometric evolution and has rarely been done up to now (see Section 3.3).

2.1.5 *Gaseous flows*

The disc is assumed to be built by accretion of gas with primordial composition. On purely phenomenological grounds, infall constitutes the most elegant and natural way to account for the G dwarf problem in the solar neighbourhood (e.g. Tinsley 1980;

Pagel 1997), but is also supported by some chemo-dynamical models of the Milky Way (Samland et al. 1997).

The infall rate $f(t,R)$ is normalized to the local disc surface density $\Sigma_{\rm T}(R)$:

$$\int_0^T f(t,R)\,{\rm d}t = \Sigma_{\rm T}(R) \tag{3}$$

where $T = 13.5\,{\rm Gyr}$ is the adopted age of the disc. The form of $f(t, R_{\rm S} = 8\,{\rm kpc})$ is adjusted to satisfy the constraint of the G dwarf metallicity distribution in the solar neighbourhood. An exponentially decreasing infall rate $f(t) \propto {\rm e}^{-t/\tau}$ with $\tau > 7\,{\rm Gyr}$ can provide a satisfactory fit to the new data (Chiapini, Matteucci & Gratton 1997 and Section 3.1.1), and we adopt here this minimal value for $\tau(R_S)$. We note that such long time-scales for the disc formation (many Gyr) are also obtained in recent chemo-dynamical models (Samland et al. 1997). To simulate the 'inside-out' formation of the disc (suggested by dynamical models, e.g. Larson 1976), the infall time-scale $\tau(R)$ is assumed to be radially dependent, taking lower values in the inner regions ($\tau = 1\,{\rm Gyr}$ at radius $R = 2\,{\rm kpc}$) and larger ones in the outer disc ($\tau = 10\,{\rm Gyr}$ at $R = 18\,{\rm kpc}$). The radial variation in the SFR efficiency and in the infall time-scale are the only parameters of the model explicitly dependent on radius.

We assume that the disc is evolving as independent one-zone rings. This (over)simplification ignores in general the possibility of radial inflows in gaseous discs, resulting e.g. by viscosity or by infalling gas with specific angular momentum different from that of the underlying disc; in both cases, the resulting redistribution of angular momentum leads to radial mass flows. The magnitude of the effect is difficult to evaluate, because of our poor understanding of viscosity and our ignorance of the kinematics of the infalling gas. Models with radial inflows have been explored in the past (Mayor & Vigroux 1981; Lacey & Fall 1985; Clarke 1989; Chamcham & Tayler 1994); at the present stage of our knowledge, introduction of radial inflows in the models would imply even more free parameters and make impossible the study of radial variation in the efficiency of the SFR.

2.2 Spectrophotometric evolution

Once the chemical evolution of a galactic zone has been calculated, its Spectrophotometric evolution can also be followed. The spectrum of the zone at time t is the sum of the individual spectra $l_\lambda(M, t - t', Z(t'))$ of stars of mass M, formed at time $t' < t$ with metallicity $Z(t')$ and still alive at time t:

$$L_\lambda(t) = \int_t \int_M \Psi(t')\Phi(M) l_\lambda(M, t - t', Z(t'))\,{\rm d}M\,{\rm d}t' \tag{4}$$

This integral can, in principle, be evaluated by integrating first either over time (isomass method) or over mass (isochrone method). The limits of the corresponding integrals are not the same in the two methods. In the first one:

$$L_\lambda(t) = \int_{M_{\rm min}}^{M_{\rm max}} \Phi(M) \left[\int_{t_{\rm inf}(Z(t'))}^{t} \Psi(t') l_\lambda(M, t - t', Z(t'))\,{\rm d}t' \right] {\rm d}M \tag{4a}$$

while in the second one:

$$L_\lambda(t) = \int_0^t \Psi(t') \left[\int_{M_{\rm min}}^{M_{\rm up}(Z(t'))} \Phi(M) l_\lambda(M, t - t', Z(t'))\,{\rm d}M \right] {\rm d}t' \tag{4b}$$

In the first case (isomass), the lower limit of the first integral (inside [ ]) is $t_{\rm inf}(Z(t')) = t - \tau_M(Z(t'))$ and represents the creation time of the star of mass M dying at time t. This limit itself depends on the integration variable t' of the first integral because of the metallicity-dependent lifetimes of stars; obviously, in that case the first integral cannot be calculated and the isomass method cannot be applied. In the second case (isochrone), the upper limit of the first integral (inside [ ]) is $M_{\rm up}(Z(t')) = M[\tau_M(Z(t')) = t - t']$, i.e. it corresponds to the heaviest star created at time t' and dying at time t; this limit does not depend on the integration variable M and the integration can always be performed. Thus, although the two methods are, in principle, equivalent when metallicity-independent lifetimes are considered, *the isochrone method is the only one applicable when metallicity-dependent lifetimes are taken into account* (as they should). We adopt the second method in this work.

Calculation of the double integral in equations (4) requires knowledge of: (a) the stellar IMF $\Phi(M)$; (b) the SFR $\Psi(t)$; (c) the metallicity $Z(t)$; and (d) the stellar spectra $l_\lambda(M,t,Z)$ for all evolutionary stages and initial metallicities.

Ingredient (a) is the same as the one adopted in Section 2.1.2, ingredients (b) and (c) are obtained self-consistently, by the adopted prescription for the SFR and the run of the chemical evolution model, and ingredient (d) is discussed in Sections 2.2.1 and 2.2.2 below.

Equation (4b) gives the composite spectrum of the stellar population of the galaxy. This spectrum is subsequently modified by ionization of the ambient gas (its ultraviolet part) and absorption by dust. The (crude) modelling of the latter process is discussed in Section 2.2.3.

2.2.1 *Stellar evolution tracks*

We adopt in this work the tracks of the Geneva group (Schaller et al. 1992; Charbonnel et al. 1996), concerning stars in the mass range $0.8 \leq M/{\rm M}_\odot \leq 120$ and in the metallicity range $Z_1 = 0.05\,{\rm Z}_\odot$ to $Z_2 = {\rm Z}_\odot$. The positions of the stars in the Hertzsprung–Russell (HR) diagram (effective temperature $T_{\rm eff}$ and bolometric luminosity L) are given, along with the corresponding ages, at equivalent points of the evolution (e.g. main-sequence turn-off, He ignition, etc.), allowing for an easy interpolation to other stellar masses and metallicities in the given range.

Stars with $M < 0.8\,{\rm M}_\odot$ and main-sequence lifetimes $\tau_{\rm MS} > 13\,{\rm Gyr}$ are always attributed their zero-age main-sequence (ZAMS) position, assuming an appropriate mass–luminosity relationship (Baraffe et al. 1998); in view of their very low ZAMS luminosity, their role is negligible in the framework of this work. For $Z < Z_1$ we adopt the tracks for $Z = Z_1$, and for $Z > Z_2$ the tracks for Z_2. This approximation has a negligible effect on the final results, since very few stars in the disc have metallicities outside that range (see Sections 3.1 and 3.2).

The metallicity dependence of the stellar tracks and lifetimes may have a considerable impact on the photometric evolution. For that reason, we present in Fig. 3 the main-sequence lifetimes, and the zero-age main-sequence $T_{\rm eff}$ and L of the adopted models for $Z = {\rm Z}_\odot$ and $Z = {\rm Z}_\odot/20$. Stars of low mass and low metallicity may be ~ 30 per cent hotter, ~ 60 per cent more luminous and have ~ 30 per cent shorter lifetimes than their more 'metallic' counterparts.

2.2.2 *Stellar spectra*

An important contribution to studies of galactic chemical evolution has recently been made by Lejeune, Cuisinier &

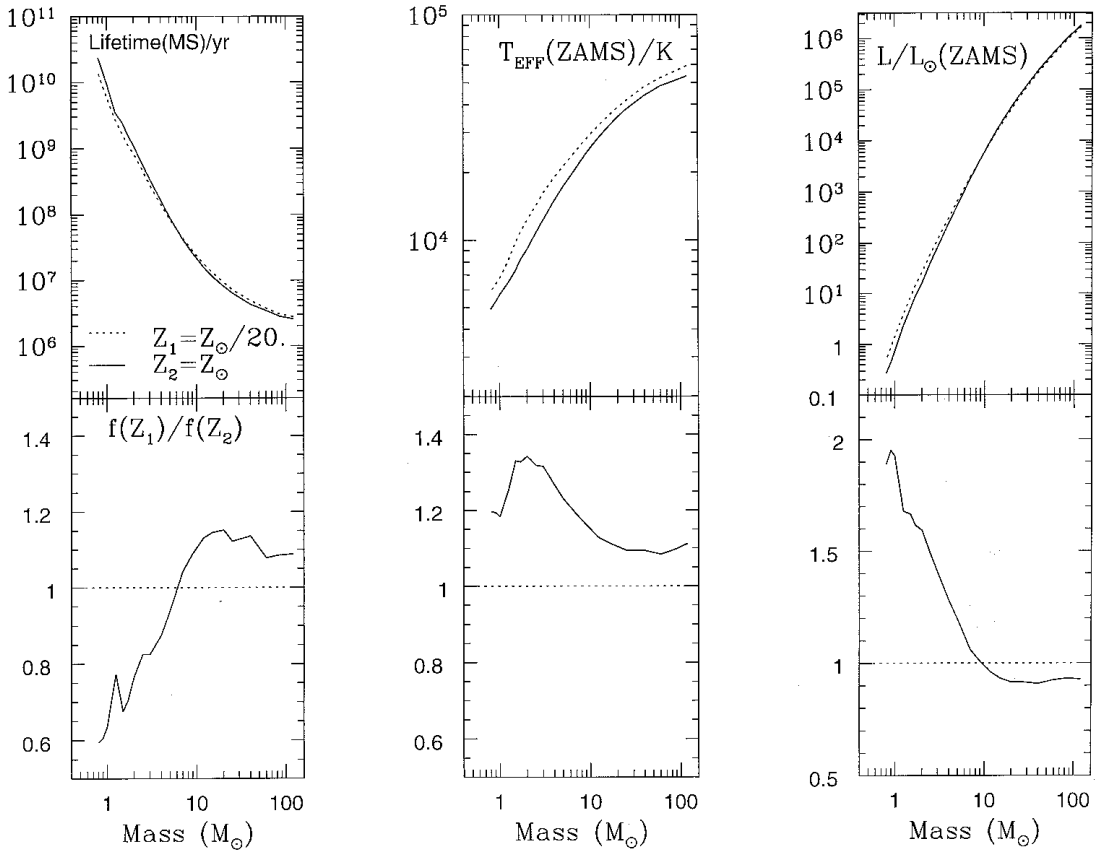

Figure 3. Comparison of main-sequence (MS) lifetimes (*left*), zero-age main-sequence (ZAMS) effective temperatures (*middle*) and luminosities (*right*) of stars with metallicity $Z_1 = Z_\odot/20$ (*dotted* curves in the *upper* panels) and $Z_2 = Z_\odot$ (*solid* curves in the *upper* panels). In the *lower* panels is displayed the ratio of the corresponding quantities $f(Z_1)/f(Z_2)$. Stars with lower metallicities are in general hotter; those of mass $< 5\,M_\odot$ are more luminous and have shorter lifetimes than their higher-metallicity counterparts. All data are from the library of the Geneva stellar evolution tracks (see Section 2.2.1).

Buser (1997). They constructed a homogeneous library of synthetic stellar spectra by compiling different sets of stellar atmosphere models published in the literature. The library covers the wavelength range from 9 nm to 160 μm with a resolution of 1 nm in the ultraviolet, 2 nm in the optical and 10 nm in the infrared. Stellar spectra are given in the three-dimensional phase space of $T_{\rm eff}$, surface gravity g and metallicity [Fe/H], and are uniformly sampled in the range $2500\,{\rm K} < T_{\rm eff} < 50\,000\,{\rm K}$, $-1 < \log(g) < 5.5$ and $-3.5 < [{\rm Fe/H}] < +1$. In the temperature range 3500 to 50 000 K the models are identical to those of Kurucz (1995). In the range 2500 to 3500 K, composite models of M giants with [Fe/H] between −1.5 and +0.5 were constructed, by connecting the Fluks et al. (1994) synthetic spectra with the Bessell et al. (1991) models. Finally, M dwarf model spectra in the range 2000 to 3500 K were selected from the grid of Allard & Hauschildt (1995). As described in Lejeune et al. (1997), these synthetic spectra have been corrected so as to reproduce empirical colour–magnitude relationships, thus eliminating the risk of theoretical errors.

The homogeneity of the library greatly facilitates the calculation of stellar luminosities l_λ, allowing an easy interpolation in stellar mass, metallicity and evolutionary stage. Magnitudes and colours are calculated in the standard photometric system *UBVRIJK* for each galactic zone.

2.2.3 *Extinction by dust*

Interstellar dust absorbs light from the stars with a wavelength-dependent efficiency and re-emits it in the far-infrared (FIR) range. The resulting extinction as a function of wavelength is difficult to evaluate from first principles (see Corradi, Beckman & Simonneau 1996 for a recent attempt, solving the full radiative transport problem in the case of a disc) and models usually adopt empirical prescriptions.

Extinction, i.e. the quantity $A_\lambda = -2.5\log(L_\lambda/L_\lambda^0)$ where L_λ^0 is the intrinsic luminosity of the stellar population calculated in equation (3) and L_λ the emerging one, depends on both the physical processes involved (absorption and scattering by dust grains) and the geometry of the source. The former is usually parametrized with the introduction of an effective optical depth τ_λ depending on the amount of dust and the absorbing and reflecting properties of grains, while the latter depends on the assumed relative distributions of stars and dust.

The effective optical depth is expressed in terms of the exctinction properties observed in the solar neighbourhood: (i) the extinction in the V band per gas surface density $(A_V/N_{\rm H})_\odot = 5.3\times10^{-22}\,{\rm mag\,cm^2}$ (Bohlin, Savage & Drake 1978) where $N_{\rm H}$ is the surface density of H (in atom $\rm cm^{-2}$); and (ii) the mean extinction curve $(A_\lambda/A_V)_\odot$, adopted here from Natta & Panagia

(1984). The dependence on metallicity is introduced by a wavelength-independent factor $(Z/Z_\odot)^s$, with $s = 1.35$ for $\lambda < 2000$ Å and $s = 1.6$ for $\lambda > 2000$ Å (adopted from Guiderdoni et al. 1998). The effective optical depth is expressed as:

$$\tau_\lambda = 0.92 a_\lambda \left(\frac{A_\lambda}{A_V}\right)_\odot \left(\frac{A_V}{N_H}\right)_\odot \left(\frac{Z}{Z_\odot}\right)^s N_H \quad (5)$$

where a_λ represents a positive contribution to the emerging radiation from light scattered by dust grains, having an albedo ω_λ. We adopt in this work the approximation of Calzetti, Kinney & Storchi-Bergmann (1994), concerning a case intermediate between isotropic scattering and purely forward scattering; it turns out that a_λ is given then by:

$$a_\lambda = h_\lambda \sqrt{1-\omega_\lambda} + (1-h_\lambda)(1-\omega_\lambda) \quad (6)$$

where h_λ is a phase factor given by:

$$h_\lambda = 1 - 0.561 \exp\left(-\frac{|\log(\lambda) - 3.3112|^{2.2}}{0.17}\right) \quad (7)$$

with λ expressed in Å. The grain albedo ω_λ in Calzetti et al. (1994) and in this work is adopted from the work of Natta & Panagia (1984). (For further discussion on the derivation of the above formulae, the reader is referred to Calzetti et al. (1994).)

The geometry of the distribution of dust is taken into account as in Xu et al. (1997), in a 'sandwich model' one half of the stars is assumed to be mixed with the layer of dust, while the other half lies on each side of this layer, the quarter behind the dust being obscured by the screen. The resulting extinction is then:

$$A_\lambda = -2.5 \log\left(0.25 + 0.5\frac{1-e^{-\mu}}{\mu} + 0.25 e^{-\mu}\right) \quad (8)$$

where $\mu = \tau_\lambda/\cos(i)$ and i is the inclination angle ($i = 0°$ for face-on galaxies). The first term in parentheses represents the contribution to the emerging luminosity from the stars in front of the dust layer, the second term from the stars mixed with dust and the third one from the stars behind the dust layer.

Extinction should, in principle, be treated with a full radiative transfer code, as e.g. in Corradi et al. (1996). They find that the effect of forward scattering is a very important one, leading to small values of extinction even for large values of the optical depth (e.g. $A_V \sim 0.1$ mag for $\tau_V \sim 4$). We are fully aware that the prescription adopted here is a very crude one (although it is being routinely adopted in many studies of that kind). For that reason we present below systematically our results for both cases: without (i.e. stellar population only) and with extinction taken into account, according to the adopted prescriptions. In a forthcoming paper we explore the consequences of the radiative transfer treatment of Corradi et al. (1996) on the absorption in various wavelengths.

3 THE EVOLUTION OF THE MILKY WAY

The Milky Way is a heterogeneous system, with at least three components (halo, bulge, disc) having very different chemical, photometric and kinematic properties. A reliable model for the evolution of the Milky Way accounting for those properties does not exist at present. In particular, it is not clear how the various components are related, e.g. whether the evolution of the halo has affected in an important way the one of the bulge or the disc (and vice versa); in fact, it seems that the halo evolution has been completely decoupled from the one of the disc, which evolved quite independently (e.g. Gilmore & Wyse 1998). Neither is it clear whether there has been significant interaction between the various parts of the disc, through large-scale gas movements in the radial direction. Despite the development of various models, all these issues are still open.

For the purposes of this work we shall adopt a very simple model for the chemical evolution of the Galactic disc, considering it as an ensemble of independently evolving, concentric, rings. In our modelling we are guided by phenomenology rather than theoretical principles and we try to construct a model that reproduces all the major observational constraints of the Milky Way with a minimum number of free parameters.

3.1 The Solar neighbourhood

3.1.1 Chemical evolution

In the Solar neighbourhood (defined as a cylinder of ~ 1 kpc radius at a distance $R_S = 8$ kpc from the Galactic centre), the main observables relevant to chemical evolution are (for a detailed discussion of these observables see PA95 and PS98; see also Table 1 for data and references and Fig. 4 for a graphical presentation of the data):

(i) The current surface densities of gas (Σ_G), stars (Σ_*) and total amount of matter (Σ_T), as well as the current star formation rate Ψ_0; a recent analysis of all available data, interpreted in the framework of a consistent mass model for the Milky Way (Mera et al. 1998), shows that there is no compelling evidence for the presence of substantial amounts of substellar objects (brown dwarfs), but a limited amount ($\Sigma_{BD} < 8\,M_\odot\,pc^{-2}$) cannot be excluded at present.

(ii) The abundances of various elements and isotopes at Solar birth ($X_{i,\odot}$) and today ($X_{i,O}$).

(iii) The age–metallicity relationship, traced by the Fe abundance of long-lived, F-type stars.

(iv) The oxygen versus Fe (O–Fe) relationship, interpreted in terms of a delayed (~ 1 Gyr) appearance of SNIa, producing most of the galactic Fe.

(v) The metallicity distribution of long-lived G-type stars (Fig. 4c), showing that very few of them were formed at [Fe/H] < -0.7 (1/5 Solar) or [O/H] < -0.5 (1/3 Solar).

(vi) The present-day mass function (PDMF), resulting from the stellar IMF and the SFR history; this observable is rarely considered in studies of the local chemical evolution (with the exception of Ferrini et al. 1994). However, the resulting theoretical PDMF constitutes an important consistency check for the adopted SFR and IMF.

The simple model described in Section 2.1 can reproduce the above constraints, as can be seen in Figs 4 and 5(a). The adopted SFR and infall rates lead to a current gas surface density of $\Sigma_G \sim 10\,M_\odot\,pc^{-2}$ and to a final stellar surface density of $\Sigma_* \sim 35\,M_\odot\,pc^{-2}$, both compatible with the observations. The final amount of stellar remnants ($\Sigma_R \sim 7\,M_\odot\,pc^{-2}$, for the sum of white dwarfs + neutron stars + black holes) is slightly smaller than the current gas amount. Models of the local chemical evolution cannot avoid producing this amount of stellar remnants, i.e. about 15 per cent of the local surface density (a different IMF would slightly change this figure).

With the adopted infall and star formation rates, a current SFR

Table 1. Main observational data for the Solar neighbourhood and results of a simple model.

Observable	Observed value	References	Computed value	Main relevant parameter in the model
Surface densities of:				
Gas	$\Sigma_G = 13 \pm 3\,M_\odot\,pc^{-2}$	1	12.0	Star formation history
Stars (visible)	$\Sigma_* = 35 \pm 5\,M_\odot\,pc^{-2}$	2	34.5	
Stars (visible + remnants)	$\Sigma_* = 43 \pm 5\,M_\odot\,pc^{-2}$	3	39.9	[Stellar IMF
Total (stars + gas)	$\Sigma_T = 51 \pm 6\,M_\odot\,pc^{-2}$	4	53.0	
				+
Gas fraction	$\sigma_G = 0.15$–0.25		0.22	infall rate
Star formation rate	$\Psi_0 = 2$–$5\,M_\odot\,pc^{-2}\,Gyr^{-1}$	5	3.2	+
Past average SFR	$\langle\Psi\rangle \sim 3\,M_\odot\,pc^{-2}\,Gyr^{-1}$		2.6	star formation law]
SNII rate	$0.02\,pc^{-2}\,Gyr^{-1}$	6	0.018	
Present-day mass function (PDMF)	Low-mass part: uncertain (flatter than $X = 1.35$)	7, 8		IMF + SFR
Abundances:				Stellar yields
At $T_0 - 4.5$ Gyr	$X_{i,\odot}$	9, 10		
	$X_{O,\odot} = 9.20 \times 10^{-3}$		7.6×10^{-3}	
	$X_{Fe,\odot} = 1.17 \times 10^{-3}$		1.1×10^{-3}	
At $T_0 \sim 13.5$ Gyr	$X_{i,0} \sim X_{i,\odot}$	11, 12		
O/Fe versus Fe/H	Decline for [Fe/H] > -1	13		SNIa rate
Age–metallicity (Z versus t)	Slow increase of Z Dispersion (?)	13		Star formation + yields
Metallicity distribution of G dwarf stars	Narrow Peaked at [Fe/H] ~ -0.1	14, 15		Infall rate
Luminosities:	$L_B = 20.0 \pm 2.0\,L_{B\odot}\,pc^{-2}$	16	26.8	Star formation history
	$L_V = 22.5 \pm 3.0\,L_{V\odot}\,pc^{-2}$	17	25.9	+
	$L_K = 68.0 \pm 23.0\,L_{K\odot}\,pc^{-2}$	18	85.36	stellar tracks stellar spectra
Colours:	$B - V = 0.85 \pm 0.15$ (0.63 ± 0.1)	16 19	0.71	Extinction

References: 1. Kulkarni & Heiles (1987); 2. Gilmore et al. (1989); 3. Mera et al. (1998); 4. Sackett (1997); 5. Rana (1991); 6. Tammann et al. (1994); 7. Scalo (1986); 8. Kroupa et al. (1993); 9. Anders & Grevesse (1989); 10. Grevesse et al. (1996); 11. Cunha & Lambert (1994); 12. Cardelli & Federman (1997); 13. Edvardsson et al. (1993); 14. Rocha-Pinto & Maciel (1996); 15. Wyse & Gilmore (1995); 16. van der Kruit (1986); 17. Pagel (1997); 18. Kent et al. (1991); 19. Robin (private communication).

$\sim 3\,M_\odot\,pc^{-2}\,Gyr^{-1}$ is obtained at $T = 13.5$ Gyr, again in agreement with observations. Those ingredients, combined with the adopted IMF and stellar yields, lead to a local metallicity close to the Solar one 4.5 Gyr ago and slightly higher today (Fig. 4b). It should be noted here that observations of CNO abundances in young stars and gas in Orion show that the metallicity of this young region is lower than Solar (Cunha & Lambert 1994; Cardelli & Federman 1997), a result that is difficult to interpret in conventional chemical evolution models (see e.g. PA95); imperfect or non-instantaneous mixing could, perhaps, help to explain this observable, as well as the scatter in the age–metallicity relationship (e.g. Coppi 1997; Thomas, Greggio & Bender 1998).

The current SNII rate in the Solar neighbourhood is found to be compatible with the estimate of Tammann, Loefler & Schroder (1994) (Fig. 8f): $2 \times 10^{-11}\,pc^{-2}\,yr^{-1}$. The SNIa rate is adjusted to reproduce the observed decline of O/Fe in the local disc (Fig. 4d). The introduction of this delayed Fe source leads to an age–metallicity relationship somewhat steeper than (but still compatible with) the observations (Fig. 4b).

The differential metallicity distribution (DMD) of G dwarfs constitutes one of the strongest constraints for the evolution of the Solar neighbourhood. It represents the number of long-lived stars per unit logarithmic metallicity interval and can be evaluated as:

$$\frac{dN_G}{d[Fe/H]} = \frac{\alpha_G \Psi(t)\,dt}{d[Fe/H]} \quad (9)$$

where $\Psi(t)$ is the SFR at time t and $dN_G = \alpha_G \Psi(t)\,dt$ is the number of G-type stars born with metallicities between [Fe/H] and [Fe/H] + d[Fe/H]; α_G is the fraction of G-type stars in the IMF. Expression (9) relates explicitly the SFR history and the age–metallicity relationship to the DMD of G dwarfs. If the latter two relationships were accurately known, the local SFR could be easily derived (Prantzos 1998a), but current observational uncertainties prevent such a derivation. As can be seen from Fig. 4(c) the local G dwarf DMD is nicely reproduced with the slow infall adopted in our model. Notice that the use of metallicity-dependent stellar lifetimes cannot solve the G dwarf problem (e.g. Bazan & Mathews 1990; Rocha-Pinto & Maciel 1997).

Finally, in Fig. 4(e) we present also the evolution of the present-day mass function (PDMF), at times 0, 0.1, 0.5, 3 and 13 Gyr from the beginning, and we compare the final result with the observed PDMF of Scalo (1986, in the mass range 1–100 $M_\odot$) and KTG93 (low-mass stars only). In the mass range $< 1\,M_\odot$ (where the shape

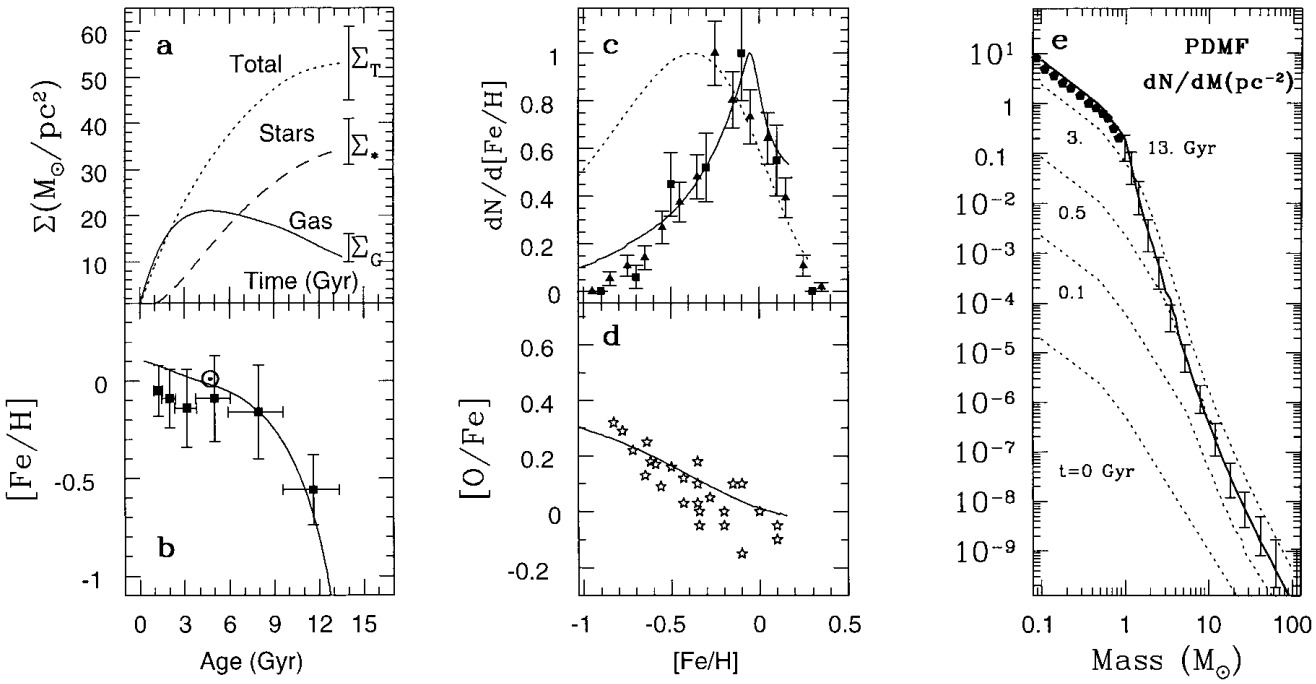

Figure 4. Results of the chemical evolution model for the Solar neighbourhood and comparison to observations (see Section 3.1.1 and Table 1 for references). (a) Surface densities of stars, gas and total amount of matter as a function of time (present-day data within vertical *error bars*); (b) age–metallicity relationship; (c) G dwarf differential metallicity distribution, with results from our model (*solid* curve) and a closed-box model (*dotted* curve) shown for comparison; (d) oxygen versus Fe relationship; (e) evolution of the present-day mass function (*dotted* curves, at various instants) and comparison of the final one (*solid* curve) to the observed PDMF of Scalo (1986, vertical *error bars* for $M > 1\,M_\odot$ stars) and of KTG93 (*filled symbols*, for low mass stars); for $M > 1\,M_\odot$ the KTG93 IMF coincides with that of Scalo (1986). Obviously, at time $t = 0$ the PDMF coincides with the adopted IMF; at $t = 13$ Gyr this is true for low-mass stars.

of the PDMF coincides with that of the IMF), the adopted IMF of KTG93 differs from the flatter ones of Scalo (1986); Gould et al. (1997) and Reid & Gizis (1997), but it is compatible with the one favoured by Haywood (1994); the Salpeter IMF is steeper than any of those IMFs. In the high-mass range, the shape of the PDMF is mainly determined by the stellar lifetimes (for small variations of the IMF slope X) and it is not surprising that the results of Scalo (1986) are recovered.

Despite the satisfactory agreement of our model with the observations, we wish to emphasize that the solution is by no means unique (see Tosi 1988), i.e. some other combinations of the input parameters may also lead to acceptable results (see Tosi 1998 for a comparison of different models). Notice, however, that the constraints are relatively tight and do not allow for a wild variation in the input parameters. In particular, the metallicity distribution strongly suggests a slow formation of the local disc; this is corroborated by the observed current local SFR (Prantzos 1998a), which is not very different from the past average one (PASFR $= \Sigma_*/T \sim 3\,M_\odot\,pc^{-2}\,Gyr^{-1}$). A very high early SFR, declining to very low current values, is not compatible with those data.

3.1.2 Photometric evolution

The set of available observational constraints concerning the photometric evolution of the Solar neighbourhood is much smaller than the corresponding one for its chemical evolution (second part of Table 1 and references therein). The local surface brightness is estimated to be $L_V = 22.5 \pm 3\,L_{V\odot}\,pc^{-2}$. Combined with the observed star surface density of $\Sigma_* = 35 \pm 5\,M_\odot\,pc^{-2}$, this leads to a local stellar mass/light ratio of $M/L_V = 1.2$–2.0 (in Solar units); if the total local surface density $\Sigma_T \sim 51 \pm 5\,M_\odot\,pc^{-2}$ is adopted instead, M/L_V is found to be ~ 1.8–2.8. Notice also the uncertainty in the local $B - V$ value, equal to 0.84 ± 0.15 (van der Kruit 1986) or to 0.63 (Robin, private communication).

The results of our model for the photometric evolution of the Solar neighbourhood appear in Fig. 5. In Fig. 5(b) appears the evolution of the M/L_V ratio where L_V is the luminosity of the stellar population calculated with metallicity-dependent stellar tracks and with no extinction taken into account. The two curves correspond to M representing either the stellar mass only or the total mass (i.e. stars + gas + stellar remnants); in both cases, the obtained value at $T = 13.5$ Gyr is on the low side of the observed range.

The effects of the metallicity dependence of the adopted stellar tracks are illustrated in Fig. 5(c) (luminosity evolution) and Fig. 5(d) (colour evolution); the results correspond again to the luminosity of the stellar population alone, i.e. without any extinction. It can be seen that the adoption of metallicity-dependent tracks leads to systematically larger B and V luminosities than for the case with $Z =$ constant $= Z_\odot$ tracks, especially towards the middle of the galactic evolution where the differences can attain 0.5 mag. Towards the end of the evolution the differences are small, since the metallicity has increased to $\sim Z_\odot$ and the tracks with $Z_\odot$ are quite appropriate. Notice that the final B and V luminosities are barely compatible with the observed local ones, but if extinction is taken into account (see next paragraph) the agreement becomes satisfactory. Notice also that the K-band luminosity is very slightly affected by these considerations. As a result, the colour evolution of e.g. B–K depends very strongly on the adopted stellar tracks. As can be seen

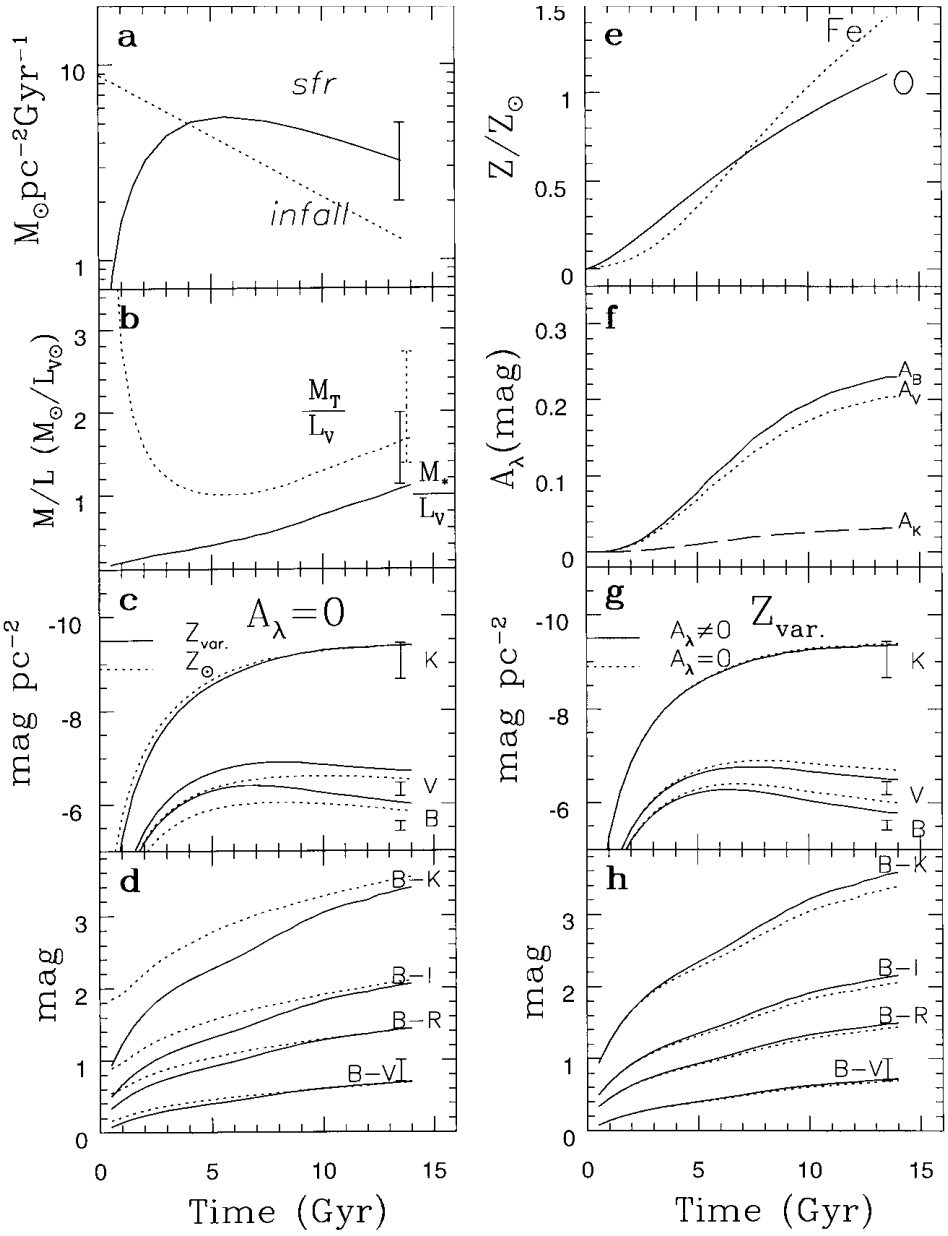

Figure 5. Results of the chemo-photometric evolution model for the Solar neighbourhood (Section 3.1.2) and comparison of the values at $T = 13.5$ Gyr to observations (with vertical *error bars*). The effects of metallicity dependence of the stellar tracks are presented in panels (c) and (d), whereas those of extinction in panels (g) and (h). (a) Star formation and infall rates; (b) M/L_V ratio for the total mass (*dotted* curve) and the stellar mass (*solid* curve); (c) surface brightness in the *K*,*V* and *B* bands, obtained with the SFR of Fig. 5(a), no extinction and stellar tracks of constant metallicity $Z_\odot$ (*dotted* curve) or variable metallicity (*solid* curve); (d) corresponding evolution of colours (*solid* curve: variable metallicity stellar tracks, *dotted* curve: tracks with $Z = Z_\odot$); (e) abundances of Fe (*dotted* curve) and O (*solid* curve) on a linear scale, the latter being adopted as tracer of metallicity for the calculation of extinction according to equation 8; (f) extinction in the *B*,*V* and *K* bands; (g) surface brightness in the *K*, *V* and *B* bands, obtained with the SFR of Fig. 5(a), stellar tracks of variable metallicity and extinction neglected (*dotted* curve) or included (*solid* curve); (h) corresponding evolution of colours (extinction neglected: *dotted* curves; extinction included: *solid* curves). *The solid curves in (g) and (h) represent our final complete model for the local photometric evolution.*

in Fig. 5(d), the early *B*–*K* is 'redder' by almost 1 mag when metallicity-independent tracks are considered. This illustrates dramatically the importance of adopting metallicity-dependent stellar tracks and calculating in a self-consistent way the photometric *and* chemical evolution of a galaxy. On the other hand, the *B*–*V* colour is very slightly affected by the metallicity dependence of the tracks; the final value [0.69 with no extinction, Fig. 5(d)] is quite close to the observed (but very uncertain!) value in the Solar neighbourhood.

On the right part of Fig. 5 are illustrated the effects of extinction on the results of our calculation. According to the adopted prescription, the optical depth depends in a sensitive way on metallicity (equation 5); one should worry then about the appropriate metallicity tracer, since O and Fe evolve in rather

different ways (Fig. 5e). Since the adopted stellar tracks of the Geneva group are parametrized by the total metallicity, dominated by oxygen, we adopt this element here as metallicity tracer in the extinction law. Another reason is that our study concerns also other Galactic regions (and, in a forthcoming paper, other spirals as well) for which there are no data concerning their Fe evolution not the SNIa rate (contrary to what happens in the Solar neighbourhood); since the evolution of the oxygen abundance is tightly related to the star formation rate, we feel that this element is a safer tracer of metallicity (at least from the theoretician's point of view).

The evolution of the extinction in various wavelengths (equation 8) appears in Fig. 5(f): it is negligible in all wavelengths in the beginning (because of low metallicity and gas amount); it is always negligible in the K band, but can reach 0.3 mag in the B and V bands. Although the metallicity increases steadily, extinction levels out at late times, because it depends also on the surface gas density, which decreases at late times (Fig. 5a). Fig. 5(g) displays the effect of extinction on luminosity: a better agreement with the current local V and (in particular) B luminosity is obtained when extinction is taken into account. Finally, Fig. 5(h) displays the corresponding evolution of various colours; $B-V$ is not affected by extinction (since both the B and V bands are affected in a similar way), while $B-K$ increases by ~ 0.25 mag.

From Figs 5(a), (g) and (h) it becomes clear that the effect of extinction on the local photometric evolution is small, mainly because of the relatively small current amount of gas. The other parameters of the model (shape of the IMF, SFR history) have a stronger impact on that evolution (see e.g. Wang & Silk 1993, for an evaluation of the impact of these parameters on chemical evolution). Notice, however, that this is not the case for inner galactic regions having larger gaseous and metal amounts (see next section).

As a final comment, we note that the effect of metallicity-dependent stellar tracks is most important in the early Galactic evolution, whereas the effects of extinction become (relatively) important only at late times.

3.2 The Milky Way disc

3.2.1 Chemical evolution

Contrary to the case of the Solar neighbourhood, the available observations for the Milky Way disc offer information mainly about its current status, not its past history. The main observables relevant to chemical evolution are (see PA95 and PS98 for a more detailed discussion; also Table 2 for data and references):

(i) The total mass of gas and stars in the disc ($M_{\rm G} \sim 6$–$8 \times 10^9\,{\rm M}_\odot$ and $M_* \sim 4$–$5 \times 10^{10}\,{\rm M}_\odot$, respectively); the total current SFR (~ 3–$6\,{\rm M}_\odot\,{\rm yr}^{-1}$) and the current supernova rates ($\sim$ 1–2 SNII century^{-1} and $\sim$ 0.2–0.4 SNIa century^{-1}, respectively, as suggested by observations of external spirals; the uncertainty on the value of the Hubble constant and on the exact spectral type of the Milky Way – Sb or Sbc – prevents us from giving a precise value). Notice that those quantities are often mentioned as constraints to (and predictions of) one-zone models of the Galaxy, assumed to reflect the evolution of the whole disc. This is obviously wrong, since the disc is a heterogeneous system, as the observed gradients suggest [see points (iii)–(vi) below]. A multizone model with different SFR histories in its various zones should be obviously used. In fact, observations of external spirals give rather the SN frequency in SNU (i.e. in number of SN per century and per $10^{10}\,{\rm L}_{B\odot}$ in Table 2); knowledge of the current L_B for the Milky Way then allows one to infer its current SN frequency. However, a successful model of the Milky Way should reproduce in a self-consistent way *both* its SN frequency and L_B luminosity.

(ii) The current gas profile, dominated by the molecular ring at Galactocentric distance $R \sim 4$–5 kpc and by H I of roughly constant surface density at distances 6–14 kpc (Dame 1993 and Fig. 2).

(iii) The stellar profile, exponentially decreasing outwards. The value of the characteristic scalelength is still under debate, but recent studies converge towards low scalelengths, around 2.5–3 kpc (Sackett 1997). A recent analysis of the *COBE* data (Freudenreich 1998) also points to a scalelength $h = 2.6$ kpc. The combination of observables (ii) and (iii) leads to a gas fraction profile steeply decreasing in the inner disc, suggesting that the star formation efficiency has been larger in those regions than in the outer disc.

(iv) The current SFR profile (traced by the surface density of pulsars and supernova remnants or the Hα emissivity profile), strongly decreasing outwards (Fig. 2 and references therein). Notice that the SFR profile does not follow the molecular or the total (molecular + atomic) one, i.e. the SFR is not simply proportional to some power of the gaseous profile.

(v) The current metallicity profile, usually traced by oxygen observed in H II regions (Shaver et al. 1983; Vilchez & Esteban 1996), young planetary nebulae (Allen, Carigi & Peimbert 1998), and B stars (Smart & Rolleston 1997; Gummersbach et al. 1998), showing a gradient of ${\rm d[O/H]} \sim -0.08\,{\rm dex\,kpc}^{-1}$.

Notice that, since there are essentially no constraints on the past history of the Milky Way disc (i.e. no age–metallicity relations or metallicity distributions are available for other regions) there is much more freedom in its modelling than in the case of the Solar neighbourhood. Still, it is meaningful to construct models, in so far as the number of parameters used is considerably smaller than the constraints (i)–(v) above.

In our previous works (PA95, PS98) we presented a simple model of that kind, i.e. one with the same physics as for the Solar neighbourhood and with a radial dependence in the star formation rate SFR(R) and the infall time-scale $\tau(R)$. As discussed in Section 2.1.1, the adopted radial dependence has a physical basis (i.e. large-scale instabilities in rotating discs for the SFR and inside-out formation of the disc for the infall time-scale τ). It turns out that with this simple parametrization the model reproduces reasonably well the constraints (i)–(v), as can be seen in Fig. 6. Among those, the gaseous profile is the most difficult to reproduce by models of that kind; we obtain a rather broad peak around 5 kpc, in rough agreement with observations. It is difficult to ask more from such a simple model, especially since other factors may have shaped the gaseous profile in the inner Galaxy (like e.g. the presence of a bar inducing radial inflows and enhancing the SFR there). Notice that this difficulty of the simple models has already been pointed out in Wang (1990).

The model also reproduces reasonably well the total current SFR and supernova rates (Table 2), as well as various other quantities. This is a rather encouraging success, since the number of new constraints is much larger than the number of new parameters. In fact, the stellar profile is essentially determined by the boundary conditions [the adopted $\Sigma_{\rm T}(R)$ profile in the normalization of equation 3], but the form of the star formation rate $\Psi(R)$ and infall time-scale $\tau(R)$ (two parameters) account then for the observed gaseous, SFR and oxygen profiles, as well as the other results in Table 2 and Fig. 6.

Table 2. Main observational data for the Milky Way disc and results of a simple model.

Observable	Observed value	References	Computed value	Main relevant parameter in the model
Total mass of:				
Gas	$M_G = 6–8 \times 10^9\,M_\odot$	1, 2, 3	8.0×10^9	Same ingredients
Stars	$M_* = 4–5 \times 10^{10}\,M_\odot$	1, 4	3.8×10^{10}	
Gas fraction	$\sigma_G \sim 0.15$		0.15	as for
Star formation:				
Current SFR	$\Psi_0 = 2–6\,M_\odot\,yr^{-1}$	1, 7	1.9	Solar
Frequency of SNII	0.55–1.0 SNU	8, 9	0.61	
Frequency of SNIa	0.12–0.23 SNU	8, 9	0.16	
				neighbourhood
Infall rate	$f < 2\,M_\odot\,yr^{-1}$	7	0.64	
				plus
Profiles:				
Gas	$\Sigma_G(R)$	1, 2		
Stars	$\Sigma_*(R) \propto e^{-R/H}$			radially dependent
	($H \sim 2.5$ kpc)	4, 5, 6, 16		
SFR	$\Psi(R)$	1, 14		SFR $\Psi(R)$
Abundances in	$X_i(R)$			Infall $f(R)$
gas and B stars	$d[O/H]/dR \sim -0.08$ dex kpc^{-1}	10, 11	−0.07	
Luminosities:	$L_B = 1.8 \pm 0.3 \times 10^{10}\,L_{B\odot}$	12	1.8×10^{10}	Same ingredients
	$L_V = 2.1 \pm 1.0 \times 10^{10}\,L_{V\odot}$	5	2.0×10^{10}	
	$L_K = 6.7 \times 10^{10}\,L_{K\odot}$	13	7.5×10^{10}	as for Solar
Colours:	$B - V \sim 0.8$	12	0.78	neighbourhood
Scalelengths:				Photometry
	$H_B = 4–5$ kpc	13	3.9	
	$H_K = 2.3–2.8$ kpc	14, 15	2.6	

References: 1. Prantzos & Aubert (1995); 2. Dame (1993); 3. Kulkarni & Heiles (1987); 4. Mera et al. (1998); 5. Sackett (1997); 6. Robin et al. (1992); 7. Pagel (1997); 8. Tammann et al. (1994); 9. Cappellaro et al. (1997); 10. Shaver et al. (1983); 11. Smart & Rolleston (1997); 12. van der Kruit (1986); 13. Kent et al. (1991); 14. Wang & Silk (1994); 15. Freudenreich (1998); 16. Ruphy et al. (1996).

The model can then be used with some confidence for making further predictions. Some of them have been analysed elsewhere: see e.g. Prantzos (1996) for the importance of the deuterium abundance profile for our understanding of the past history of the disc, or Prantzos et al. (1996) on the evolution of the CO isotopic profiles. In Fig. 6 we present two more predictions of the model concerning (a) the evolution of the metallicity gradients in the disc and (b) the surface density of compact objects (white dwarfs, neutron stars and black holes) as a function of Galactocentric distance.

The evolution of the metallicity gradient is an important issue in studies of the evolution of galactic discs (see e.g. Köppen 1994 and references therein). In particular, the flattening of the metallicity profile supports the idea of inside-out formation of the disc (since the inner regions arrive at the endpoint of their evolution more rapidly than the outer ones). In the case of our model, this evolution is clearly seen in Figs 6(a)–(c), where the gaseous, stellar and SFR profiles are given at three times (1, 5 and 13.5 Gyr respectively). Unfortunately, the existing abundance data on stars and planetary nebulae of various ages do not allow at present conclusions on the behaviour of the metallicity profile on an observational basis (see Molla et al. (1997) for a thorough discussion of the data and the associated uncertainties). The recent works of Molla et al. (1997) and Allen et al. (1998) conclude that the O abundance profile should become flatter with time and that it should evolve very little in the past ~ 6 Gyr, on the basis of models not very different from ours. We confirm these conclusions, as can be seen in Fig. 6(e). Also, in agreement with Molla et al. (1997) we find that the Fe abundance profile is steeper than the one of oxygen at any age (Fig. 6(f)); this is the result of the enhanced ratio of SNIa to SNII in the inner disc, resulting from the adopted prescription for the SNIa rate (see Section 2.1.4). As already stressed in PA95, the evolution of the O versus Fe abundance profiles is crucial to our understanding of the past SNIa history in other regions of the Galactic disc.

The last two panels of Fig. 6 display the final profiles of the surface densities of stellar remnants, by mass (Fig. 6g) and by number (Fig. 6h), respectively. As already discussed in Section 3.1.1, the local surface density of stellar remnants is found to be slightly lower than the corresponding gaseous one. Comparison to Fig. 6(a) shows that in the inner disc stellar remnants dominate the gas (i.e. inside ~ 5 kpc). In Fig. 6(h) it is seen that in the inner Galaxy number densities of stellar remnants (always dominated by white dwarfs) can reach $\sim 100\,pc^{-2}$. These numbers, resulting from our model, may have important implications for: (a) the resulting M/L_V profile (see Section 3.3.2); (b) statistics of experiments concerning microlensing events in the direction of the Galactic bulge (e.g. Han & Chang 1998 and references therein); or (c) the detection of neutron stars and black holes in binary systems (e.g. Romani 1998; Bethe & Brown 1998). The

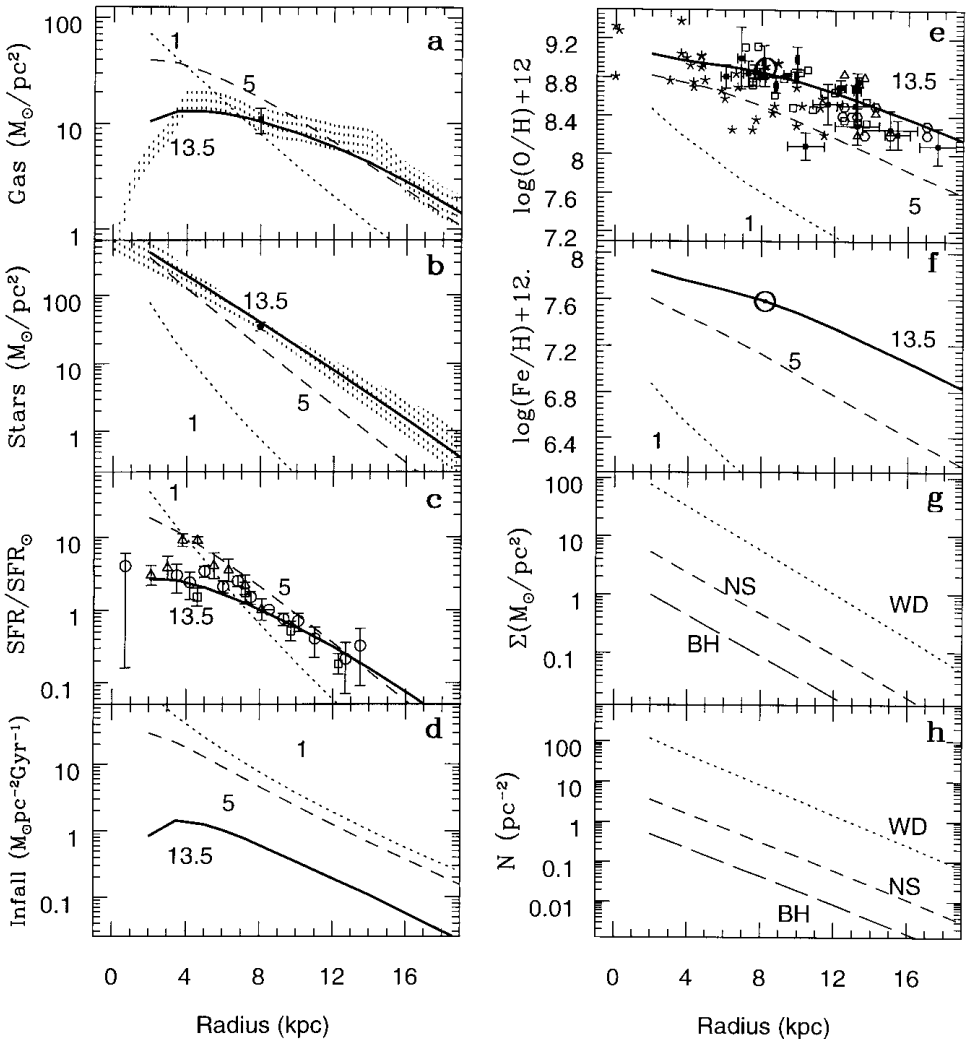

Figure 6. Results of the chemical evolution model for the Milky Way disc (Section 3.2.1) and comparison to observations (see Table 2 for references). (a) Gas profile at 1 Gyr (*dotted* curve), 5 Gyr (*dashed* curve) and 13.5 Gyr (*thick solid* curve) and comparison of the latter to observations of the current gaseous profile (*grey* area, normalized to the local gas surface density, within *error bars*); (b) stellar profile at 1 Gyr (*dotted* curve), 5 Gyr (*dashed* curve) and 13.5 Gyr (*thick solid* curve) and comparison of the latter to observations of the current stellar profile (*grey* area, within two exponential discs of scalelengths 2.2 and 2.6 kpc, respectively, and normalized to the current local star surface density, within *error bars*); (c) star formation rate, normalized to its current value at $R_S = 8$ kpc at 1 Gyr (*dotted* curve), 5 Gyr (*dashed* curve) and 13.5 Gyr (*thick solid* curve) and comparison of the latter to observations (see Fig. 2 and references therein for observational data); (d) profile of the infall rate at 1 Gyr (*dotted* curve), 5 Gyr (*dashed* curve) and 13.5 Gyr (*thick solid* curve); (e) oxygen abundance profile at 1 Gyr (*dotted* curve), 5 Gyr (*dashed* curve) and 13.5 Gyr (*thick solid* curve) and comparison of the latter to observations; (f) iron abundance profile at 1 Gyr (*dotted* curve), 5 Gyr (*dashed* curve) and 13.5 Gyr (*thick solid* curve); (g) current surface densities (by mass) of white dwarfs (WD, *dotted* curve), neutron stars (NS, *short-dashed* curve) and black holes (BH, *long-dashed* curve); (h) current surface densities (by number) of white dwarfs (*dotted* curve), neutron stars (*short-dashed* curve) and black holes (*long-dashed* curve).

resulting total current numbers in our model are: $\sim 10^{10}$ white dwarfs, 5×10^8 neutron stars and $\sim 5 \times 10^7$ black holes in the Galaxy. The numbers for neutron stars and black holes are lower by a factor of ~ 2 than the corresponding ones of Timmes et al. (1996), one of the reasons being the use of the Salpeter IMF in that work compared to the more realistic KTG93 IMF in our model.

3.2.2 Photometric evolution

As in the case of the Solar neighbourhood, the set of photometric data for the Milky Way disc is smaller (and more uncertain) than the corresponding one for chemical evolution (Table 2). In particular, there is considerable uncertainty about the scalelength in the various wavelengths; it is clear, however, that scalelengths are larger in the shorter wavelengths (e.g. $\sim$ 4–5 kpc in the *B* band versus $\sim$ 2.3–3 kpc in the *K* band). One of the main results of this section concerns precisely this issue.

The evolution of the luminosity profile in several wavelengths and of the associated colour profiles appears in Fig. 7, for three different epochs, 1, 5 and 13.5 Gyr, so that a direct comparison is possible with the corresponding profiles of gas, stars, SFR and metallicity (Fig. 6). Our calculations are performed with metallicity-dependent stellar tracks and results are displayed with and without extinction.

The luminosity profiles clearly reflect the inside-out formation of the disc, one of the basic ingredients of our model: in all wavelengths the disc is smaller and more compact in early times. The *K*-band profile reflects better the stellar profile of Fig. 6(b)

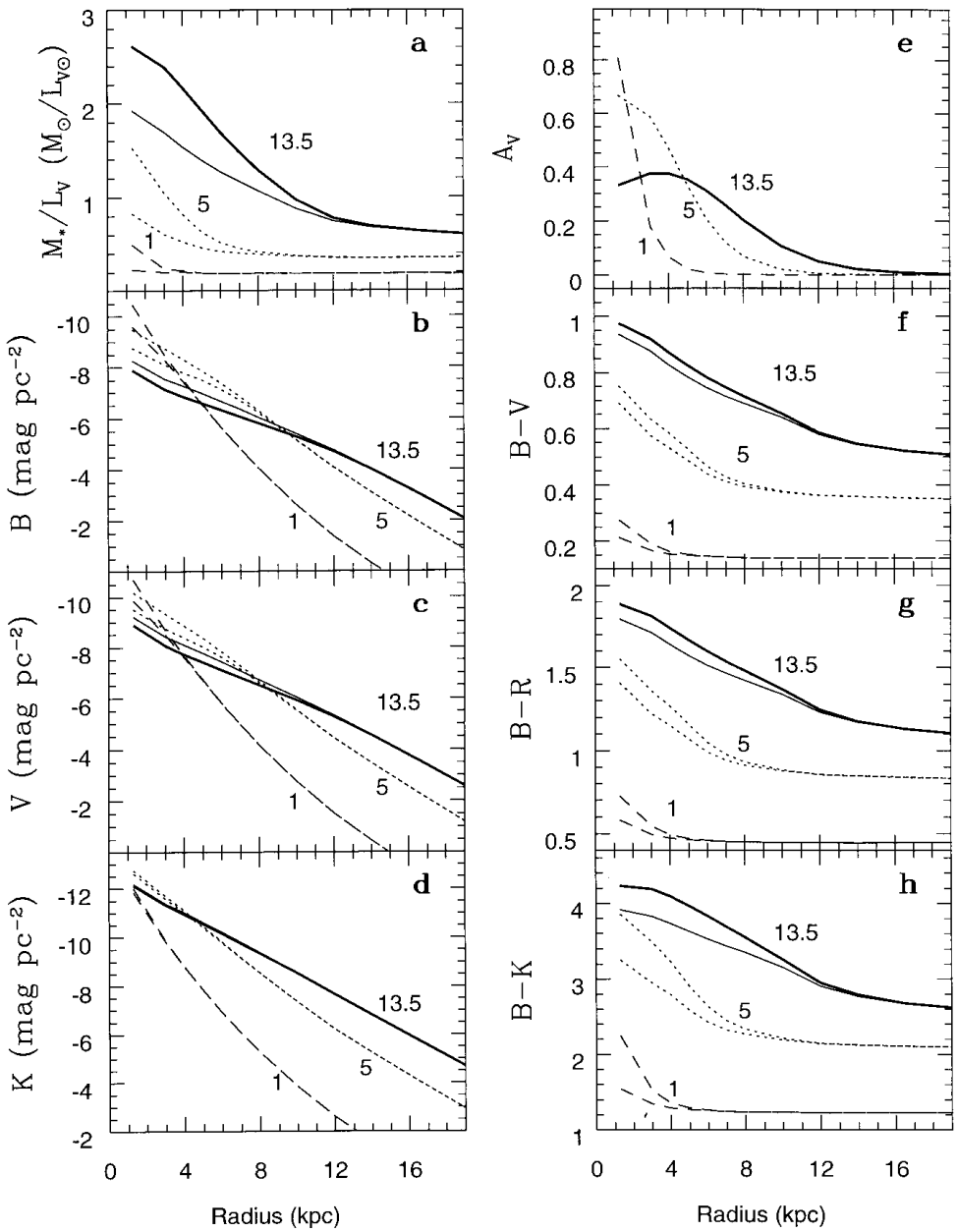

Figure 7. Results of the chemo-photometric evolution model for the Milky Way disc (Section 3.2.2) with metallicity-dependent stellar tracks. In each panel, three curves are given, corresponding to profiles at times $t = 1$ Gyr (*dashed* curve), 5 Gyr (*dotted* curve) and 13 Gyr (*thick solid* curve), respectively; bifurcation of the curves (mostly in the inner disc) corresponds to extinction neglected (upper part of the bifurcation in the surface brightness profiles, lower part in the colour profiles and M/L_V ratio) or included (lower part in the surface brightness profiles, upper part in the colour profiles and M/L_V ratio). (a) Stellar M/L_V ratio; (b) B surface brightness (the final exponential disc has a scalelength of $H_B \sim 3.9$ kpc but breaks down outside ~ 13 kpc; (c) V surface brightness; (d) K surface brightness (the final exponential disc has a scalelength of $H_K \sim 2.6$ kpc, i.e. shorter than the B disc, in fair agreement with observations; (e) extinction in the V band; (f) evolution of $B - V$ colour profile; (g) evolution of $B - R$ colour profile; (h) evolution of $B - K$ colour profile. *In all the figures, the thick solid curve presents our final complete model*, i.e. with extinction taken into account. It is clear that extinction enhances but does not create colour gradients, especially at late times.

than the shorter wavelengths; its scalelength increases to a final value of ~ 2.6 kpc, in fair agreement with the observationally deduced one (Table 2). On the other hand, the B profile is generally flatter, in particular in the inner disc, and follows closely (albeit not perfectly) the SFR profile (Fig. 6c); both profiles reflect the young stellar population and flatten in the inner disc at late times because of the exhaustion of gas supply in that region. The final profile of L_B is exponential, with a scalelength ~ 4 kpc between 3 and 13 kpc, i.e. for about three scalelengths. Outside 13 kpc the final B profile steepens, as does the corresponding SFR profile (Fig. 6c).

The stellar M/L_V profile (Fig. 7a) has a uniform value ~ 0.2 (in solar units) at $t = 1$ Gyr; its value rises more rapidly in the inner disc (where it reaches a value of ~ 2 at 13.5 Gyr), than in the outer disc. As with extinction and colour profiles (see next paragraphs) the final M/L_V profile is very flat outside ~ 13 kpc. The reason is that, in the inner disc, a large number of the stars emitting in the V band are created early on and are dead by $t = 13.5$ Gyr,

contributing to M but not to L_V. In the outer disc, most of those stars are created relatively late (because of the inside-out star formation) and are still shining.

Extinction (Fig. 7e) plays some role in the inner disc, where A_V can reach ~ 0.4 mag (compared to ~ 0.2 mag in the Solar neighbourhood; see Fig. 5f). Contrary to the Solar neighbourhood, where A_V remains approximately constant in the past ~ 5 Gyr (since the effect of gas depletion is compensated by a small increase in metallicity), in the inner disc A_V *decreases* with time, since the important gas depletion is not compensated by a corresponding metallicity increase (metallicity saturates in the inner disc at late times, as seen in Fig. 6e).

In Figs 7(f)–(h) it can be seen that colour gradients are established early on in the inner disc and propagate outwards. Extinction modifies these profiles slightly (especially the $B-K$ one), more at intermediate times than at the end of the evolution (for reasons explained in the previous paragraph). However, we find that extinction is not the main factor in shaping those gradients, in agreement with the analysis of Kuchinski et al. (1998) for the discs of spiral galaxies. The final colour profile presents an important gradient, extending up to 12–13 kpc. This is because, inside that radius, there are important differences in the star formation time-scales between e.g. 2–3 kpc and 6–7 kpc; inner regions have considerably older stellar populations than outer ones. However, outside the 12-kpc radius the disc is still young (star formation happens late because of the long infall time-scales) and colour gradients are not established. The main point of this section concerns precisely the prediction of colour gradients in the inner disc, related to the existence of different scalelengths for the various wavelength bands. These features are a direct consequence of the inside-out formation scheme adopted here, on the basis of some theoretical arguments. A 'uniform' formation of the disc (i.e. with the same time-scale of star formation everywhere) would lead to similar scalelengths in all wavelengths and would create very small colour and metallicity gradients. On the other hand, extinction may certainly enhance colour gradients, but to a relatively small degree (at least with the prescriptions adopted in this work). The available data for the Milky Way allow only a very limited check of these ideas, but the large sample of observations concerning external spiral galaxies offers the opportunity for a detailed comparison; these issues are explored in a forthcoming paper (Boissier & Prantzos 1999).

3.3 Milky Way versus Solar neighbourhood

In studies of the photometric (and, sometimes, chemical) evolution of spiral galaxies with one-zone models, calibration is often made to the Solar neighbourhood observables, i.e. it is assumed that the local disc evolution is representative of the average Milky Way disc evolution. In this section we check this assumption, in the framework of our model. We calculate total (extensive) quantities $Q_{\rm T}$ for the disc as:

$$Q_{\rm T}(t) = \int_0^{R_{\rm G}} 2\pi q(R,t) R \, {\rm d}R \tag{10}$$

where $q(R,t)$ is any quantity expressed in units of surface density ($\rm pc^{-2}$) and $R_{\rm G}$ is the outer Galactic radius. With this equation we obtain L_λ^0 when integrating the stellar luminosity alone, and L_λ when integrating the luminosity after correction for extinction at each radius. The 'integrated' extinction is then $A_\lambda = -2.5\log(L_\lambda/L_\lambda^0)$. Magnitudes and colours of the whole disc are computed from the integrated spectrum. We also calculate average (intensive) quantities as e.g. abundances. In this case, the average galactic value $\langle X_i \rangle$ is

$$\langle X_i(t) \rangle = \frac{\int_0^{R_{\rm G}} 2\pi X_i(R,t) \Sigma_{\rm gas}(R,t) R \, {\rm d}R}{\int_0^{R_{\rm G}} 2\pi \Sigma_{\rm gas}(R,t) R \, {\rm d}R} \tag{11}$$

The results are plotted in Fig. 8, where the Solar neighbourhood evolution (left part) is compared to that of the Milky Way disc (right part). The final average Fe and O abundances in the gas of the disc (Fig. 8A) are similar to those in the Solar neighbourhood (Fig. 8a), but their history is different: early on, the average disc abundances are dominated by the inner Galaxy, which evolves more rapidly than the Solar neighbourhood; thus, the average disc metallicity increases more rapidly than that of the local disc early on, whereas at late times the trend is reversed. The same behaviour is shown by the mass in stars and the SFR (Figs 8b and B).

An issue of considerable interest is the one of the SFR versus gas amount. In the case of the Solar neighbourhood, the current/maximum ($q_{\rm now}/q_{\rm max}$) ratio is ~ 0.7 for the gas surface density and ~ 0.5 for the SFR density (as expected from the $\Psi \propto \Sigma_{\rm G}^{1.5}$ law adopted locally); both the gas and the SFR have a broad maximum around 5–6 Gyr. In the case of the Milky Way, the corresponding ratio is ~ 0.8 for the total gas and ~ 0.20 for the total SFR, i.e. those two global quantities do not obey the local Schmidt law; besides, their maxima do not coincide, being at $\sim$ 3–4 Gyr for the gas and $\sim$ 1–2 Gyr for the SFR. The reason for this behaviour is, of course, the non-linearity of the adopted SFR law, as a result of both the exponent (1.5) and the R^{-1} factor; both these factors enhance the SFR efficiency early on in the inner disc, where there is a lot of gas infalling rapidly. At late times, even if the total amount of gas is the same, it is distributed differently. A large part of the total SFR comes now from the outer regions (favoured by their larger aera), where the SFR efficiency is small. In view of the importance of that topic, we make a more detailed analysis in Section 3.4, where a comparison to observational data of external spirals is performed.

In Figs 8(c) and (C) it can be seen that there are also important differences between the Solar neighbourhood and the Milky Way concerning the evolution of extinction. In the former case, A_B and A_V rise steadily, while in the latter they undergo an early maximum (owing to the combined large amounts of gas *and* metals in the inner disc) and then decline steadily, since the gas in the inner regions is consumed and its metallicity barely increases; the outer regions play no role in the overall extinction, in view of their low column densities and metallicities.

The integrated luminosity of the Galaxy (Fig. 8D) evolves strongly in the first several Gyr, being dominated by the inner disc. After that period, the K luminosity stays nearly constant (most of the Galactic stars are already formed), while the B and V luminosities decrease slowly [because of the declining total SFR of Fig. 8(B), although they do not follow it perfectly]. At $R_S = 8$ kpc (Fig. 8d), luminosities rise and decline more slowly. This difference in time-scales is also present in the colour evolution (Figs 8e and E): while the Solar neighbourhood reddens steadily from $t = 0$ to the present time, the integrated colours have an evolution that is more rapid at early times and slower at late times.

The SN rates for the whole disc (Fig. 8F) are expressed in SNU (SN century^{-1} per 10^{10} $\rm L_{B\odot}$). The SNII frequency (in SNU) is high early on and decreases steadily, because L_B does not follow exactly the SFR (stars contributing to L_B are not as short-lived as those exploding as SNII). The results at $T = 13.5$ Gyr for both

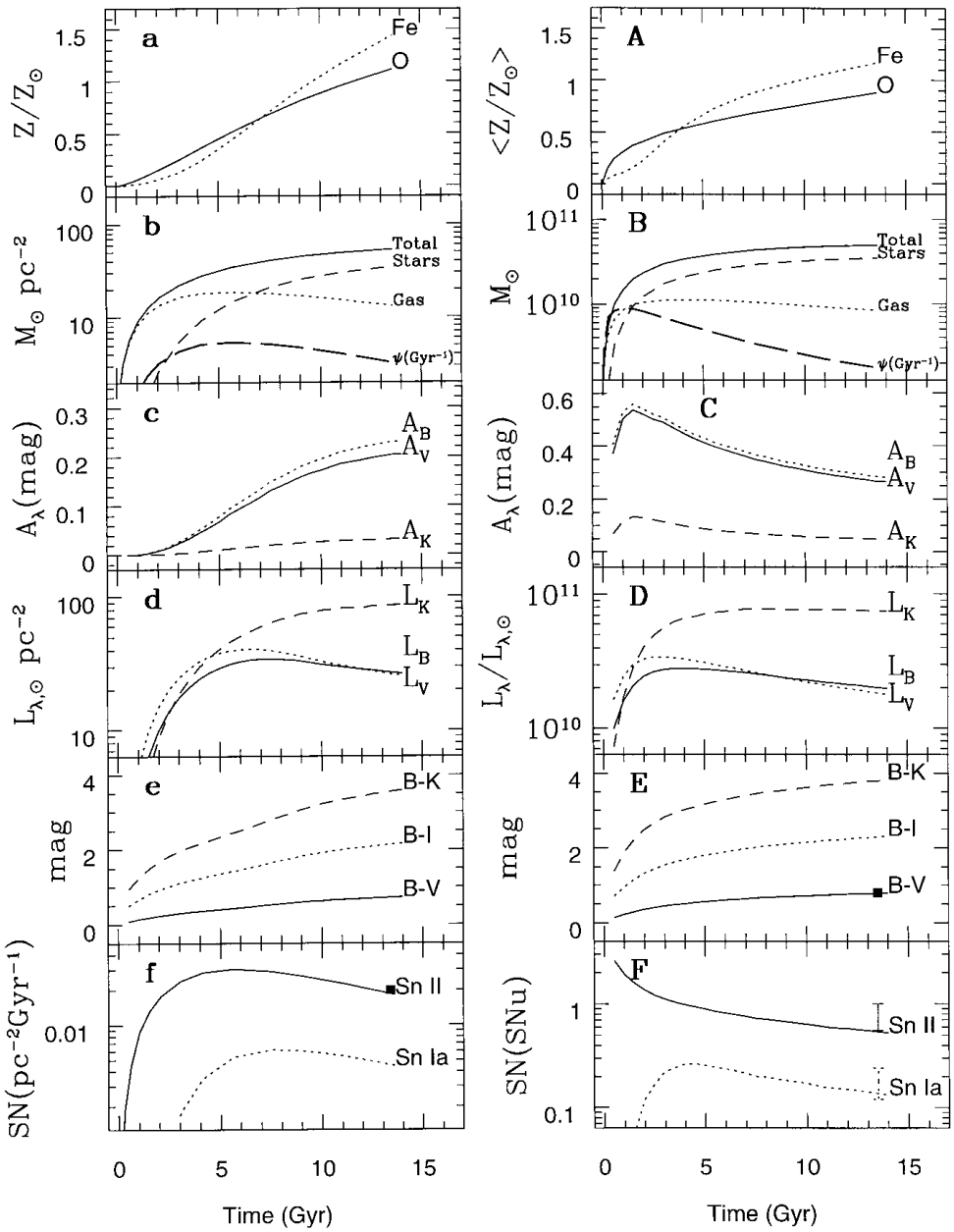

Figure 8. Comparison of the results for the chemo-photometric evolution of the Solar neighbourhood (on the left, see Section 3.1) and that of the Milky Way (on the right, see Section 3.3 for the calculation of integrated or average properties). (a) and (A): evolution of Fe and O abundances on a linear scale; (b) and (B): evolution of gaseous, stellar and total mass (in $M_\odot\,pc^{-2}\,Gyr^{-1}$ on the left, in $M_\odot$ on the right), as well as of star formation rate (corresponding units per Gyr); (c) and (C): evolution of extinction in the *B*, *V* and *K* band; (d) and (D): evolution of *B* (*dotted*), *V* (*solid*) and *K* (*dashed*) luminosities, with extinction included; (e) and (E): evolution of $B-K$, $B-I$ and $B-V$ colours (with extinction); (f) and (F): evolution of supernova rates; the local ones (f) are expressed in units of $pc^{-2}\,Gyr^{-1}$, while the total ones (F) in SNU, i.e. the total SN rates (per century) are divided by the *B*-band luminosity, expressed in $10^{10}\,L_{B\odot}$. For observational data (*filled squares* or *vertical error bars* at $T = 13.5$ Gyr) see Table 2 and references therein.

SNII and SNIa are closer to the rates reported (Tammann et al. 1994; Cappellaro et al. 1997) for Sb rather than Sbc galaxies and for low rather than high values of the Hubble constant (both factors, i.e. the Sb type and low Hubble value, lead to lower deduced frequencies in SNU).

Finally, the evolution of the M/L_V ratios, obtained by dividing the stellar and total mass of the disc (Fig. 8B) by the L_V luminosity (Fig. 8D), is shown in Fig. 9. Both quantities increase steadily and more rapidly than in the case of the Solar neighbourhood (Fig. 5b), because most of the disc mass resides in the inner Galaxy, which evolves more rapidly than the local disc. Also, the M/L_V ratio depends somewhat on the calculated amount of extinction (up to 45 per cent in the early evolution and to 20 per cent towards the end).

In summary, the overall evolution of the Milky Way disc bears little similarity to that of the Solar neighbourhood (or to any other region for that matter). Because of the non-linearity of the SFR efficiency with Galactic radius, evolution is dominated by the inner disc at early times. At late times, most of the 'action' takes place in the outer disc, which dominates extensive quantities (equation 10) that follow the SFR; at those late times, intensive quantities (equation 11) receive important contributions from the

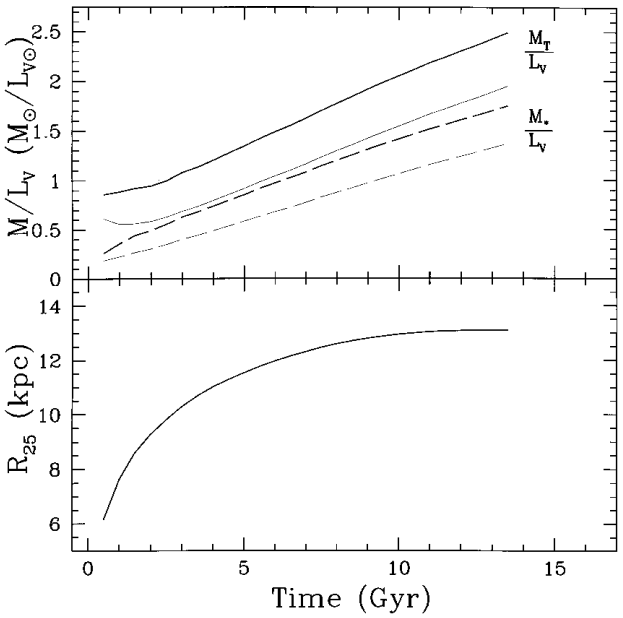

Figure 9. *Upper panel*: Evolution of the galactic M/L_V ratio for the total mass (*solid* curves) and the stellar mass (*long dashed* curves), with extinction neglected (i.e. stellar population alone, *thin* curves) or included (*thick* curves). *Lower panel:* Evolution of the isophotal radius R_{25}, at which the B-band surface brightness is equal to 25 mag arcsec^{-2}.

whole disc. This behaviour of spiral discs resulting from our model has important implications for the observations of external spirals, at both low and high redshift.

3.4 The average SFR in the Milky Way and normal spirals

The behaviour of local versus global SFR, briefly discussed in the previous section, is better illustrated in Fig. 10. The local SFR in each Galactic zone obeys the adopted Schmidt law (upper panel), but with considerably different efficiencies (because of the R^{-1} factor). However, the global SFR versus total gas amount (middle panel in Fig. 10) has a completely different behaviour: for the same gas amount, very different values of the SFR are found. It is true that the high values concern the early evolution (before the first 2 Gyr), where the SFR is dominated by the innermost regions of the disc and the adopted SFR prescription is probably not valid (since there are no spiral arms inside ~ 2 kpc, at least in the case of the current Milky Way). When the first 2 Gyr are neglected, we find a relationship between global SFR and gas amount (thick part of the curve in Fig. 10, middle), which corresponds to a slope of ~ 4, i.e. $\mathrm{SFR_T} \propto M_\mathrm{G}^4$; this simply reflects the highly non-linear behaviour of the adopted SFR prescription, but *has no physical meaning* and cannot be used in any model of chemical evolution. Indeed, the important conclusion of this analysis is that, even if a Schmidt-type SFR law is introduced locally, any radial dependence of the SFR efficiency will make the global SFR of a disc deviate considerably from this law. In other words, *it is impossible to model spiral galaxies by one-zone models with a fixed relationship between SFR and gas amount*. This would make some sense only if there were no radial variation in the SFR efficiency, but in that case *no gradients of abundances or colours would be obtained*, contrary to observational evidence.

A more physical insight is obtained by analysing the behaviour of *average* quantities, i.e. average SFR density versus average gas density; both averages are made over some portion of the disc area. In a recent study concerning normal spiral galaxies and starbursts Kennicutt (1998) divides total SFR and Σ_G by $\pi R_{25}(B)^2$, where $R_{25}(B)$ is the radius at which the surface brightness in the B band is equal to 25 mag arcsec^{-2}. The evolution of $R_{25}(B)$ in our model is given in Fig. 9 (lower panel): it increases in the first 6 Gyr up to $R_{25} \sim 13.5$ kpc (because of the adopted infall and SFR laws) and stays roughly constant afterwards. By dividing the model total SFR and Σ_G by $\pi R_{25}(B)^2$, we are able to compare directly our results to the data of Kennicutt (1998). His data for normal spirals are plotted also in Fig. 10 (lower panel), but we increased his gas surface densities (concerning the sum of $\mathrm{H_2} + \mathrm{H\,I}$) by 40 per cent ($= 1.0/0.7$) to account for a contribution of 30 per cent He by mass (to compare directly with our results). Our model curve (after the first 0.5 Gyr) lies well within the data points, i.e. the *absolute* values of the average SFR during the Milky Way evolution correspond fairly well to observations of external spirals. Also, after the first 0.5 Gyr we find a unique slope $N = 1.7$ in the average SFR versus gas surface density relationship. This value is to be compared with the values derived by Kennicutt (1998): $N = 1.29 \pm 0.18$ for a conventional least-squares fit to his data and $N = 2.47 \pm 0.39$ for a bivariate least-squares regression, taking into account uncertainties in both the SFR and the gas density. Kennicutt (1998) concludes that '… any Schmidt type law in these galaxies should be regarded as a very approximate parametrization at best'. We showed here that the adopted local Schmidt law leads to an average SFR compatible with available data for external spirals. However, this does not imply that the adopted $N = 1.5$ is the real value of the local Schmidt law; our result only implies that, when combined with the R^{-1} factor for the SFR efficiency, the $N = 1.5$ exponent leads to results that are compatible with all available observables in the Milky Way and with observations of the average SFR versus gas density in other spirals. Some other combination (i.e. a different N and a different radial dependence of the SFR efficiency) could, perhaps, lead also to acceptable results.

4 CONCLUSIONS

We have developed a model computing coherently the chemical and spectrophotometric evolution of spiral discs. The model makes use of up-to-date input ingredients (i.e. stellar IMF and yields, metallicity-dependent stellar lifetimes, evolutionary tracks and spectra) and considers the galactic disc as an ensemble of independently evolving concentric rings built by infall of gas of primordial composition. Its main ingredient is a radially dependent SFR $\Psi(R) \propto \Sigma_\mathrm{G}^{1.5} R^{-1}$, based on both empirical data (the $\Sigma_\mathrm{G}^{1.5}$ part) and theoretical arguments (the R^{-1} part). In fact, we show here (Section 2.1.3 and Fig. 2) that the adopted SFR law, when applied to the gaseous profile of the Milky Way, gives results that compare fairly well with the observed SFR profile in our Galaxy. The model is then applied to the Milky Way evolution and the main results can be summarized as follows:

(i) The main observational features of the Solar neighbourhood and the Milky Way disc are fairly well reproduced, with the simple assumptions of a slow formation of the local disc (in time-scales of many Gyr, in order to explain the observed local G dwarf metallicity distribution) and a radial variation in the efficiency of

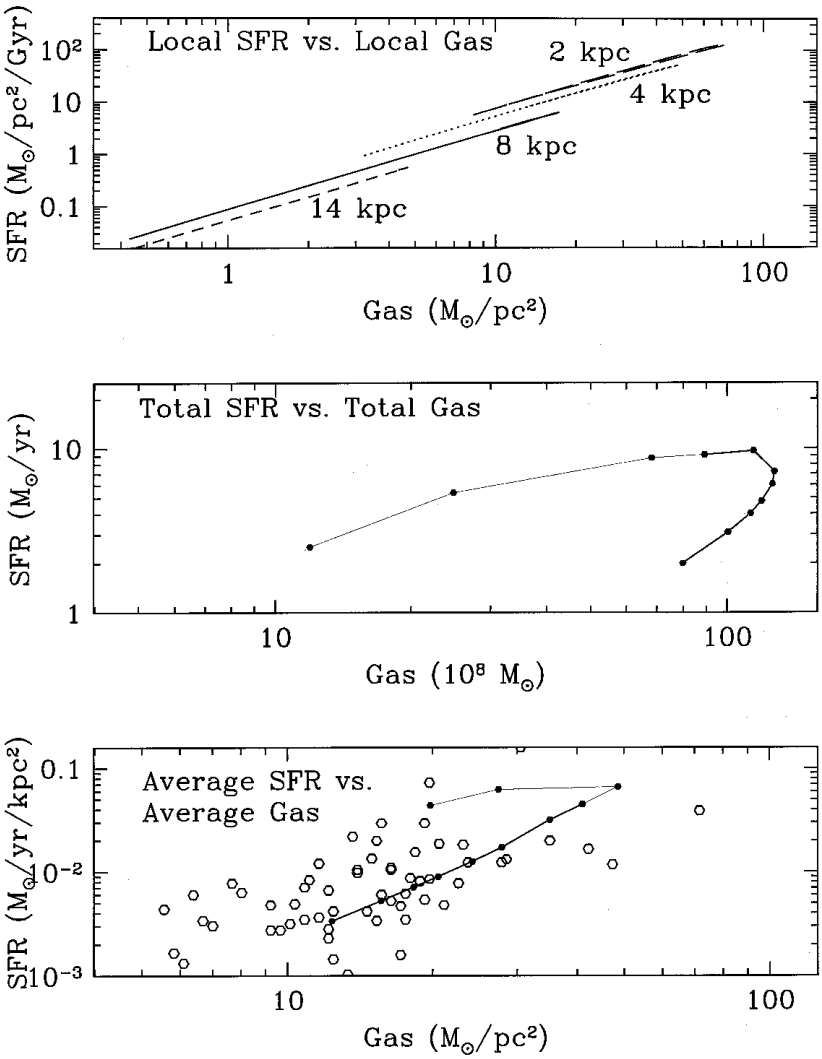

Figure 10. *Upper panel*: Local relationship between SFR and gas surface densities for four zones of our model (*curves*) during the galactic evolution; for each zone, a unique Schmidt law with slope 1.5 is recovered, but the shift between the curves indicates that the R^{-1} factor increases the SFR efficiency in the inner regions. *Middle panel:* Relationship between the total SFR and gas amount of the disc; evolution takes place from left to right in this diagram and points mark various instants in time (0.01, 0.1, 0.5, 1.0, 2.0, 4.0, 5.5, 7.5, 9.0, 11.0 and 13.5 Gyr, respectively). The local Schmidt law is not recoverd globally, because of the non-linearity of the SFR across the disc (see the discussion in Section 3.3). *Lower panel:* Relationship between the average SFR and average gas surface density in the disc; the quantities of the previous panel are divided by πR_{25}^2, where R_{25} is the radius at which $\mu_B = 25$ mag arcsec^{-2}. Results (*solid* curve with points marking several instants in time) are compared to observations in external spirals (*open* symbols); the data are from Kennicutt (1998), but the given amount of hydrogen ($H_2 + H\,I$) has been increased by 40 per cent, to take He into account, so as to be directly comparable with our results.

star formation (to obtain the observed gas and abundance gradients).

(ii) The evolution of the abundance gradients is not really constrained by observations at present. In our model, abundance gradients are predicted to flatten with time and finally to saturate in the inner disc (in agreement with a few previous works on that topic). Also, the adopted prescription for the rate of SNIa (major Fe producers) reproduces successfully a local observable (the decline of O/Fe with Fe/H in the Solar neighbourhood) and predicts a gradient of Fe/H steeper than the one of oxygen at all times (Section 3.2.1).

(iii) The predicted current SNII rate in the Solar neighbourhood is in fair agreement with observations (2×10^{-11} core collapse SN pc^{-2} yr^{-1}; Tammann et al. 1994), showing that our choice of SFR and IMF are mutually consistent; this is also corroborated by the fact that the model reproduces fairly well the local present-day mass function, something rarely considered in analogous studies (Section 3.1.1). More importantly, we obtain the total current rate of SNII and SNIa expressed in SNU, i.e. by calculating both the supernovae rates and the evolution of the blue luminosity of the Galaxy. The results are on the low side of (but compatible with) observations of external galaxies (Section 3.3 and Table 2).

(iv) We calculate the surface density profiles of the various stellar remnants (dominated always by white dwarfs). We find that currently in the Solar neighbourhood their contribution is smaller than the mass of gas, while in the inner disc it is much larger and can reach ~ 20 per cent of the stellar surface density (Section 3.2.1). We find that there should currently exist $\sim 10^{10}$ white dwarfs, $\sim 5 \times 10^8$ neutron stars and $\sim 5 \times 10^7$ black holes in the Galaxy (within a factor of ~ 2, depending on the IMF and the mass of the disc). On the total, the Galactic mass of compact objects is comparable to the one of gas, i.e. each contributes for ~ 7–8×10^9 M$_\odot$ or ~ 12–15 per cent of the mass of the disc. These results may have important implications for the statistics of

microlensing events towards the bulge, or for the detection of Galactic neutron stars and black holes in binary systems.

(v) The use of metallicity-dependent stellar tracks, lifetimes and spectra, along with a full chemical evolution model, is mandatory in studies of the photometric evolution of galaxies (especially of systems with large metallicity variations in long time-scales, such as spirals, see Section 3.1.2). We also show that, when metallicity-dependent lifetimes are used (as they should!) only the isochrone method is applicable when calculating the luminosity evolution of a galaxy (Section 2.2).

(vi) The adopted scheme of star formation in the disc leads naturally to different scalelengths in the various photometric bands (shorter in the red and longer in the blue), in fair agreement with observations of the Milky Way disc for which we obtain: $H \sim 2.6$ kpc in the K band and $H \sim 4$ kpc in the B band (Section 3.2.2). Also, it produces Galactic discs that are much more compact in the past, an important result in view of current studies of galaxy evolution at high redshifts.

(vii) For the same reason, colour gradients are obtained, first in the inner disc, then propagating outwards. We find no colour gradients in the outer disc, which is formed relatively late in that scheme, so that there is no time for colour gradients to be established there (Section 3.3.2). Moreover, we find that extinction enhances but does not really create colour gradients (at least with the adopted prescription).

(viii) The evolution of various parameters in the solar neighbourhood (stars, gas, abundances, luminosities, etc.) does not match the corresponding evolution (of average or global quantities) of the whole disc. This is due to the non-linearity of the adopted star formation law as a function of galactocentric radius. In particular, the early evolution of the Galaxy (dominated by the inner disc) is more rapid and the late evolution slower than the one of the Solar neighbourhood. This implies that one-zone models reproducing the evolution of the Solar neighbourhood cannot be taken as representative of the evolution of the Milky Way as a whole (Section 3.3).

(ix) The adopted scheme of star formation (main ingredient of the model) compares fairly well to observations of average SFR versus gas surface density of external spirals. Notice that such a comparison can be made only in the framework of chemo-photometric models since the R_{25} radius is required for the averaging (see Section 3.4).

We notice that the photometric results of our model depend strongly on the quality of the adopted stellar tracks and spectra. In that respect, the use of the now available homogeneous set of these ingredients presents a great improvement. However, the Geneva tracks include neither the horizontal branch (negligible in the context of this work) nor the thermally pulsing asymptotic giant branch phase [potentially more important, but certainly not able to invalidate our conclusions in points (vi) and (vii)].

Finally, the success of the model does not necessarily imply its correctness. It suggests however that there may be a grain of truth in the overall picture, which should be further tested against a larger mass of observational data, concerning spiral galaxies at low and high redshifts. Work is in progress along these directions.

REFERENCES

Allard F., Hauschildt P., 1995, ApJ, 445, 433
Allen C., Carigi L., Peimbert M., 1998, ApJ, 494, 247
Anders E., Grevesse N., 1989, Geochim. Cosmochim. Acta, 53, 197
Arimoto N., Yoshii Y., Takahara F., 1992, A&A, 253, 21
Baraffe I., Chabrier G., Allard F., Hauschildt P., 1998, A&A, 337, 403
Bazan G., Mathews G., 1990, ApJ, 354, 64
Bessell M., Brett J., Scholz M., Wood P., 1991, A&AS, 89, 335
Bethe H., Brown G., 1995, ApJ, 445, L129
Bethe H., Brown G., 1998, astro-ph/9805355
Boesgaard A.-M., King J., Deliyannis K., Vogt S., 1999, AJ, 117, 492
Bohlin R., Savage B., Drake J., 1978, ApJ, 224, 132
Boissier S., Prantzos N., 1999, MNRAS, submitted
Bruzual A., Charlot S., 1993, ApJ, 405, 538
Calzetti D., Kinney A., Storchi-Bergmann T., 1994, ApJ, 429, 582
Cappellaro E., Turatto M., Tsvetkov D., Bartunov O., Pollas C., Evans R., Hamuy M., 1997, A&A, 322, 431
Cardelli J., Federman S., 1997 in Gorres J., Mathews G., Shore S., Wiecher M., eds. Nuclei in the Cosmos IV. Elsevier, Amsterdam, p. 31
Carigi L., 1996, Rev. Mex. Astron. Astrofis., 32, 179
Chamcham C., Tayler R., 1994, MNRAS, 266, 282
Charbonnel C., 1998, in Friedly D. et al., eds, ASP Conf. Ser., Abundance Gradients as a Diagnostic Tool for Galaxy Evolution, Astron. Soc. Pac., San Francisco, p. 157
Charbonnel C., Meynet G., Maeder A., Schaerer D., 1996, A&AS, 115, 339
Chiapini C., Matteucci F., Gratton R., 1997, ApJ, 477, 765
Clarke C., 1989, MNRAS, 238, 283
Contardo G., Steinmetz M., Fritze-von Alvesleben U, 1998, ApJ, 507, 497
Coppi G., 1997, ApJ, 487, 704
Corradi R., Beckman J., Simonneau E., 1996, MNRAS, 282, 1005
Cunha K., Lambert D., 1994, ApJ, 426, 170
Dame T., Holt S., Verter F., 1993, Back to the Galaxy, 267Am. Inst. Phys., New York
Dopita M., Ryder S., 1994, ApJ, 430, 163
Dwek E., 1998, ApJ, 501, 643
Edvardsson B., Anderssen J., Gustafsson B., Lambert D., Nissen P., Tomkin J., 1993, A&A, 275, 101
Ferrini F., Molla A., Pardi M., Diaz A., 1994, ApJ, 427, 745
Firmani C., Hernandez X., Tutukov A., 1996, A&A, 403, 414
Fluks M., Plez B., The P., De Winter D., Westerlund B., Steenman H., 1994, A&AS, 105, 311
Freudenreich H., 1998, ApJ, 492, 495
Gilmore G., Wyse R., 1998, AJ, 176, 748
Gilmore G., Wyse R, Kuijken K., 1989 in Beckman J., Pagel B., eds. Evolutionary Phenomena in Galaxies, Cambridge Univ. Press, Cambridge, p. 172
Gilmore G., Parry I., Ryan S., (eds), 1998, The Stellar Initial Mass Function. Astron. Soc. Pac., San Francisco
Gizis J., Reid I., 1999, AJ, 117, 508
Gould A., Bacall J., Flynn C., 1997, ApJ, 482, 913
Grevesse N., Noels A., Sauval J., 1996, in Holt S., Sonneborn G., eds., ASP Conf. Ser. Vol. 99, Cosmic Abundances. Astron. Soc. Pac., San Francisco, p. 13
Guibert J., Lequeux J., Viallefond F., 1978, A&A, 68, 1
Guiderdoni B., Rocca-Volmerange B., 1987, A&A, 186, 1
Guiderdoni B., Hivon E., Bouchet R., Maffei B., 1998, MNRAS, 295, 877
Gummersbach C., Kaufer A., Schäffer D., Szeifert T., Wolf B., 1998, A&A, 338, 881
Gusten R., Mezger M., 1983, Vistas Astron., 26, 159
Han C., Chang K., 1998, MNRAS, 299, 1040
Haywood M., 1994, A&A, 282, 444
Iben I., Tutukov A., 1984, ApJ, 284, 719
Israelian G., Garcia-Lopez R., Rebolo R., 1998, ApJ, 507, 805
Jimenez R., Padoan P., Matteucci F., Heavens A., 1998, MNRAS, 299, 123
Kennicutt R., 1989, ApJ, 344, 685
Kennicutt R., 1998, ApJ, 498, 541
Kent S., Dame T., Fazio G., 1991, ApJ, 378, 131
Köppen J., 1994, A&A, 281, 26
Kroupa P., 1998, in Rebolo R. et al., eds, ASP Conf. Ser. Vol. 134, Brown Dwarfs and Extrasolar Plantes. Astron. Soc. Pac., San Francisco, p. 483

Kroupa P., Tout C., Gilmore G., 1993, MNRAS, 262, 545 (KTG93)
Kuchinski L., Terndrup D., Gordon K., Witt A., 1998, AJ, 115, 1438
Kulkarni S., Heiles C., 1987, in Hollenbach D., Thronson H., eds, Interstellar Processes. Kluwer, Dordrecht, p. 87
Kurucz R., 1995, CDROM, private communication to Lejeune et al. 1997
Lacey C., Fall M., 1985, ApJ, 290, 154
Larson R., 1976, MNRAS, 176, 31
Lejeune T., Cuisinier F., Buser R., 1997, A&AS, 125, 229
Lilly S. et al., 1998, ApJ, 500, 75
Lyne A., Manchester R., Taylor J., 1985, MNRAS, 213, 613
Marigo P., Bressan A., Chiosi C., 1996, A&A, 313, 545
Massey P., 1998, in Aparicio E. et al., eds, Stellar Astrophysics for the Local Group. Cambridge Univ. Press, Cambridge, p. 95
Massey P., Johnson K., Degioia-Eastwood K., 1995, ApJ, 454, 151
Matteucci, François, 1989, MNRAS, 239, 885
Matteucci F., Greggio L., 1986, A&A, 154, 279
Mayor M., Vigroux L., 1981, A&A, 98, 1
Mera D., Chabrier G., Schaeffer R., 1998, A&A, 330, 953
Molla M., Ferrini F., Diaz A., 1997, ApJ, 475, 519
Natta A., Panagia N., 1984, ApJ, 287, 228
Nomoto K., Iwamoto K., Kishimoto N., 1997, Sci, 276, 1378
Onihishi T., 1975, Prog. Theor. Phys., 53, 1042
Pagel B., 1997, Nucleosynthesis and Galactic Chemical Evolution, Cambridge Univ. Press, Cambridge
Prantzos N., 1994, A&A, 284, 477
Prantzos N., 1996, A&A, 310, 106
Prantzos N., 1998a, in Prantzos N., Tosi M., von Steiger R., eds, Primordial Nuclei and their Galactic Evolution. Kluwer, Dordrecht, p. 225
Prantzos N., 1998b, in Friedly D. et al., eds., ASP Conf. Ser, Abundance Gradients as a Diagnostic Tool for Galaxy Evolution. Astron. Soc. Pac., San Francisco, p.171
Prantzos N., Aubert O., 1995, A&A, 302, 69 (PA95)
Prantzos N., Silk J., 1998, ApJ, 507, 229 (PS98)
Prantzos N., Aubeat O., Audouze J., 1996, A&A, 309, 760
Rana N., 1991, ARA&A, 29, 129
Reid I. N., Gizis J., 1997, AJ, 113, 2246
Renzini A., Voli A., 1981, A&A, 94, 175
Robin A., Crézé M., Mohan V., 1992, A&A, 265, 32
Rocha-Pinto H., Maciel W., 1996, MNRAS, 279, 447
Rocha-Pinto H., Maciel W., 1997, MNRAS, 325, 523
Romani R., 1998, A&A, 333, 583
Ruiz-Lapuente P., Canal R., Iseru J., 1997, Thermonuclear Supernovae. Kluwer, Dordrecht
Ruphy S., Robin A., Epchtein N., Copet E., Bertin E., Fouque P., Guglielmo F., 1996, A&A, 313, L21
Sackett P., 1997, ApJ, 483, 103
Salpeter E., 1955, ApJ, 121, 161
Samland M., Hensler G., Theis C. H., 1997, ApJ, 476, 544
Scalo J., 1986, Fundam. Cosm. Phys., 11, 1
Scalo J., 1998, preprint, astro/ph-9811341
Schaller G., Schaerer D., Maeder A., Meynet G., 1992, A&AS, 96, 269
Shaver P., McGee R., Newton L., Danks A., Pottasch S., 1983, MNRAS, 204, 53
Smart S., Rolleston W., 1997, ApJ, 481, L47
Steinmetz M., Muller E., 1994, MNRAS, 276, 549
Talbot R. Jr, Arnett D., 1975, ApJ, 197, 551
Tammann G., Loefler W., Schroder A., 1994, ApJS, 92, 487
Thielemann K. F., Nomoto K., Yokoi K., 1986, A&A, 158, 17
Thielemann K. F., Nomoto K., Hashimoto M., 1996, ApJ, 460, 408
Thomas D., Greggio L., Bender R., 1998, MNRAS, 296, 119
Thorsett S., Chakrabarty D., 1999, ApJ, 512, 288
Timmes F., Woosley S., Weaver T., 1995, ApJS, 98, 617
Tinsley B., 1980, Fundam. Cosm. Phys., 5, 287
Tosi M., 1988, A&A, 197, 33
Tosi M., 1998, in Prantzos N., Tosi M., von Steiger R., eds, Primordial Nuclei and their Galactic Evolution. Kluwer, Dordrecht, p. 207
Tsujimoto T., Yoshii Y., Nomoto K., Shigeyama T., 1995, A&A, 302, 704
van der Kruit P., 1986, A&A, 157, 230
Vilchez J., Esteban C., 1996, MNRAS, 280, 720
Wang B., Silk J., 1993, ApJ, 406, 580
Wang B., Silk J., 1994, ApJ, 427, 759
Wang Z., 1990, ApJ, 360, 529
Woosley S., Weaver T., 1995, ApJS, 101, 181 (WW95)
Wyse R., Gilmore G., 1995, AJ, 110, 2771
Wyse R., Silk J., 1989, ApJ, 339, 700
Xu C., Buat V., Boselli A., Gavazzi G., 1997, A&A, 324, 32

This paper has been typeset from a TEX/LATEX file prepared by the author.